Geochimica et Cosmochimica Acta 366 (2024) 250–266

Contents lists available at ScienceDirect

Geochimica et Cosmochimica Acta

journal homepage: www.elsevier.com/locate/gca

Polycyclic aromatic hydrocarbons in tropical Australian stalagmites: a framework for reconstructing paleofire activity

Elena Argiriadis [a,b,*], Rhawn F. Denniston [c], Stefania Ondei [d], David M.J.S. Bowman [d], Giulia Genuzio [a,b], Huong Quynh Anh Nguyen [e,k], Jamie Thompson [f,l], Mattia Baltieri [b], Jonathan Azenon [g], John Cugley [h], David Woods [i], William F. Humphreys [j], Carlo Barbante [a,b]

[a] Institute of Polar Sciences, National Research Council (CNR-ISP), Via Torino 155, 30172 Venice, Italy
[b] Department of Environmental Sciences, Informatics and Statistics, Ca' Foscari University, Via Torino 155, 30172 Venice, Italy
[c] Department of Geology, Cornell College, 600 First Street Southwest, Mount Vernon, Iowa 52314-1098, United States
[d] Fire Centre, School of Natural Sciences, University of Tasmania, Sandy Bay, Tasmania 7001, Australia
[e] Department of Chemistry, Cornell College, 600 First Street Southwest, Mount Vernon, Iowa 52314-1098, United States
[f] Department of Biology, Macalester College, 1600 Grand Avenue, St. Paul, MN 55105-1899, United States
[g] Department of Biology, Cornell College, Mount Vernon, Iowa 52314-1098, United States
[h] Australian Speleological Federation, Perth, Australia
[i] Department of Environment and Science, Queensland Parks and Wildlife Service, Townsville, Queensland, Australia
[j] Western Australian Museum, Perth, Australia
[k] Department of Chemistry, Northwestern University, 2145 Sheridan Road, Evanston, IL 60208, United States[1]
[l] Department of Periodontics, University of Iowa College of Dentistry, 801 Newton Road, Iowa City, Iowa 52242, United States[1]

ARTICLE INFO

Associate editor: Ann Pearson

Original content: Polycyclic Aromatic Hydrocarbons in tropical Australian stalagmites: a framework for reconstructing paleofire activity - Research data (Original data)

Keywords:
Stalagmites
PAH
Paleofire
Caves
Speleothems
Organic matter
Australia

ABSTRACT

Human activity and climate change are altering natural rates and intensities of wildfire, but the scale and extent of burning prior to the modern era are poorly understood. Paleofire activity may be reconstructed using a variety of records (e.g., charcoal in lake sediments, burn scars on tree rings), but these are not available in all environmental settings. Here we investigate the utility of a novel paleofire proxy: trace pyrogenic organic compounds in stalagmites. Polycyclic aromatic hydrocarbons (PAHs) are linked to burning of biomass and are transported downward through soil and bedrock by infiltrating rainwater and incorporated into stalagmites in underlying caves where they are preserved. In order to test links between the stalagmite PAHs and fire above the cave, we performed a series of experiments using PAH distributions at KNI-51, a shallow cave located in tropical Western Australia, where bushfire is a regular occurrence. First, the possibility of surface contamination was evaluated by measuring PAH abundances and distributions in sequential digestions and by considering other possible additional sources, such as regional oil and gas fields or proximal combustion of fossil fuels. Second, PAHs were measured in soils above the cave and in sediments from the stalagmite chamber floor as possible sources of these organic compounds, and at near annual resolution in three aragonite stalagmites to evaluate the degree of deposition and conservation. Third, possible non-pyrogenic sources of organic compounds were evaluated through alkane distribution and specific m/z ratios. Fourth, signal replication of PAHs was tested in two coeval stalagmites. Fifth, satellite-mapped fire scars were used to examine the relationship between stalagmite PAH abundances and proximity of burning to the cave.

The results support the hypothesis that PAHs in KNI-51 stalagmite carbonate reflect paleofire activity within 3 km of the cave, and thus that stalagmites can serve as an important new high resolution proxy for landscape-scale fire activity. Given that karst is present in many fire-prone environments, and that stalagmites can be precisely dated and may grow continuously for millennia, the potential utility of a stalagmite-based paleofire proxy is high.

* Corresponding author.
E-mail addresses: elena.argiriadis@cnr.it, elena.argi@unive.it (E. Argiriadis).
[1] Present address.

https://doi.org/10.1016/j.gca.2023.11.033
Received 26 June 2023; Accepted 30 November 2023
Available online 5 December 2023

1. Introduction

Fire both reflects and drives environmental change across a spectrum of spatial and temporal scales (Bowman et al., 2009; Lasslop et al., 2019). Variations in climate and land use practices in recent decades have resulted in marked shifts in fire activity, including the occurrence of catastrophic fires such as the 2019–20 "black summer" bushfire season in eastern Australia and the recent severe fires across many parts of the western United States, Canada and Europe. Understanding the complexities involved in fire-ecosystem-climate feedbacks benefits from a knowledge of past fire dynamics, particularly during intervals of distinct human activity and/or climatic mean states. However, while reconstructions of burning prior to the instrumental era have been developed using charcoal and chemical biomarkers in lacustrine and marine sediments (Lynch et al., 2007; Argiriadis et al., 2018) and ice cores (Kehrwald et al., 2010), as well as from fire scars on tree rings (Margolis et al., 2022), the availability of these proxies is limited in many settings, including the fire-prone tropical savannas of northwestern Australia.

Speleothems (cave formations including stalagmites) are a widely used paleoclimate archive given that they can grow continuously for thousands of years, resist alteration, be precisely dated, and provide high resolution paleoenvironmental information. Stable isotopes of oxygen and carbon, along with select trace elements, are the primary chemical markers used in speleothems for paleoclimate reconstruction (Lachniet, 2009; Fairchild and Treble, 2009; Cisneros et al., 2021). The study of organic compounds in speleothems is less well developed, despite the fact that they hold the potential to preserve paleoenvironmental signals unattainable by inorganic compounds (Wynn and Brocks, 2014; Blyth et al., 2016; Campbell et al., 2023).

Paleofire reconstruction from speleothems is a novel and rapidly growing research field, as demonstrated by recent studies evidencing peaks in select trace elements (McDonough et al., 2022), and in trace organic levoglucosan (Homann et al., 2022) in stalagmites that correspond to fire activity. Polycyclic aromatic hydrocarbons (PAHs) have rarely been examined in stalagmites (Perrette et al., 2008; Homann et al., 2023), and Argiriadis et al. (2019) presented a method for the refined analysis of PAHs in stalagmites. PAHs are primarily related to combustion of biomass at the land surface and are carried downward by infiltrating water into caves where they are incorporated into speleothems (Sun et al., 2019), thereby creating the potential for stalagmites to capture environmental conditions and events, including fire, occurring over the cave.

The present work aims to assess the potential of stalagmites to serve as high resolution paleofire records by investigating the nature, distribution, and origins of PAHs in aragonite stalagmites from the tropical Australian cave KNI-51. The thin soils, shallow depth of the cave, and strong seasonality associated with the region's monsoonal climate minimize homogenization of chemical signals, and the fast growth rates of the stalagmites allow for extremely high (near annual) temporal resolution of PAH analyses. In addition, the remote location of the cave reduces the risk of contamination from anthropogenic emissions while the high fire frequency allows for a high production rate of pyrogenic compounds. Finally, satellite imagery provides detailed mapping of recent fire activity that can be compared against PAH measurements from recently deposited stalagmite material. The development of a stalagmite paleofire proxy holds enormous potential given the location of karst in many fire-sensitive regions, including tropical and temperate Australia, as well as Indonesia, Borneo, Madagascar, the western United States, and the Amazon basin.

Connecting fire activity above a cave to organic compounds in stalagmites requires understanding their source, distribution, transport, and preservation. Organic matter in stalagmites may be of autochthonous or allochthonous origin, and several different sources/mechanisms within or outside the cave environment can contribute to cave organic matter composition, including transport by suspension in water or air, dissolution in water, or through deposition of animal feces. Organic matter composition reflects the typology and activity of plant and microbial communities, together with phenomena related to climate, and natural disturbances including fire (Ramseyer et al., 1997; Blyth et al., 2008). Depending on the complexity of the soil and karst system, transport mechanisms of organic matter from the land surface into underlying caves can also affect organic matter deposition in caves, and thus also in speleothems. For instance, caves characterized by rapid infiltration typically have a higher content of organic matter than those with slower infiltration. The turnover rate of organic matter in soils must also be considered, since it introduces a time lag between organic matter production and its deposition in stalagmites, and is dependent, in part, on the thickness of the soil above the cave (Blyth et al., 2008). In addition, leaching differs according to the chemical characteristics of transported organic matter: more soluble (hydrophilic) substances (e.g., amino acids or polysaccharides) are readily leachable but also more biodegradable, while hydrophobic components (e.g., lipids) are less soluble but more resistant to degradation (Blyth et al., 2016, Blyth and Frisia, 2008).

This study focuses on stalagmites as reservoirs for PAHs, organic molecules composed of two or more fused aromatic rings formed through incomplete combustion of organic materials. According to fuel and combustion conditions, a wide range of PAHs can be produced (Oros and Simoneit, 2001). PAHs are generally characterized by a high persistence in the environment and low solubility and low abundance in natural waters (Countway et al., 2003). Among soil organic matter main components, low molecular weight PAHs are more likely associated with humins, while high molecular weight congeners are associated with black carbon contained in char, charcoal, and soot from natural fires, land clearing, crop residue burning, and fossil fuel combustion (Ukalska-Jaruga et al., 2019). Soil PAHs are, for the most part, adsorbed onto organic matter-specific sites and nanostructures that limit their biodegradation and bioavailability (Yang et al., 2010).

Immediately after fires of moderate intensity (200–400 °C), abundances of light (LMW) and medium molecular weight (MMW) PAHs are elevated in burnt soils, particularly naphthalene and phenanthrene and other 2- to 4-ring compounds, while high molecular weight PAHs (HMW) are rare to absent (see Table 1 for PAH weight classification and abbreviations used in the text) (Rey-Salgueiro et al., 2018). HMW PAHs

Table 1
List of PAH compounds and abbreviations used in this study classified by molecular weight.

Name	Abbreviation	Mol. weight (g mol^{-1})	Weight class
Naphthalene	NAP	128	LMW
Acenaphthylene	ACY	152	LMW
Acenaphthene	ACE	154	LMW
Fluorene	FLU	166	LMW
Anthracene	ANT	178	MMW
Phenanthrene	PHE	178	MMW
Fluoranthene	FLA	202	MMW
Pyrene	PYR	202	MMW
Benzo(*a*)anthracene	BaA	228	MMW
Chrysene	CHR	228	MMW
Retene	RET	234	MMW
Benzo(*b*)fluoranthene	BbF	252	HMW
Benzo(*k*)fluoranthene	BkF	252	HMW
Benzo(*e*)pyrene	BeP	252	HMW
Benzo(*a*)pyrene	BaP	252	HMW
Perylene	PERY	252	HMW
Indeno(1,2,3-*cd*) pyrene	IcdP	276	HMW
Benzo(*ghi*)perylene	BghiP	276	HMW
Dibenzo(*ah*) anthracene	DahA	278	HMW

are generally only produced at temperatures in excess of ~500 °C and thus are associated with fossil fuel combustion or very intense fires of woody material (Wang et al., 2017). The persistence of PAH compounds at the soil surface is also dependent on their volatility: concentrations of naphthalene (LMW) in soils were shown to return to pre-fire concentrations 5–9 months after a fire as a result of volatilization and degradation (Kim et al., 2011). This time period can be markedly shortened by leaching of ash during heavy rainfall events, such as are associated with monsoons, in which case pre-fire PAH abundances can be restored in 2–3 months (Vergnoux et al., 2011; Kim et al., 2011; Choi, 2014). Thus, in the shallow soils overlying cave KNI-51, PAHs resulting from fires are not expected to linger for multiple years on the land surface, as volatilization, degradation, and mechanical erosion (primarily by run-off) limit the availability of PAHs over time. However, little time is available for PAHs produced by fires occurring in the eight-month dry (April to November) - particularly the late dry (September to November) - season to be lost to volatilization before wet season monsoon rains transport these compounds into the cave. Field leaching rate is affected by several factors and is enhanced for compounds associated with dissolved organic matter (Wilcke, 2000), while soils with low total organic carbon (TOC) and low clay content show less capacity to retain PAHs.

Once transported by infiltrating waters into underlying caves, PAHs can be incorporated into speleothem carbonate, and thus the potential exists for their presence/absence and molecular weight distribution to record fire activity over the cave through time. To date, only three published studies report extraction of PAHs from stalagmites (Perrette et al., 2008; Argiriadis et al., 2019; Kaal et al., 2021). Perrette et al. (2008) analyzed samples of a calcite stalagmite in southeastern France formed in a deep cave overlain by a thick and well-developed soil containing elevated concentrations of PAHs associated with a long history of human activity. Temporal trends and compositions of PAHs in the stalagmite did not track soil stratigraphy, the overall type or abundance of humic substances included within the stalagmite, or the land-use history of the overlying surface. Instead, the authors ascribed the observed distribution of PAHs within the stalagmite to complex carbon reservoir effects occurring within the karst-soil system, each part of which responded differently to biodegradation and eluviation by infiltrating fluids. Thus, the lack of paleoenvironmental information from PAHs obtained in this study reflects the complex nature of the site's soil, bedrock, and infiltration pathways. Kaal et al. (2021) focused on the sources of organic matter in stalagmites from a cave in northern Spain. The few unsubstituted PAHs (parent compounds with no functional groups attached) that were detected (naphthalene, fluorene, and phenanthrene) were attributed primarily to pyrogenic organic matter, namely charcoal and soot, as residues of incomplete combustion, possibly from anthropogenic fires in the cave. However, the dominant source of organic matter in this cave was associated with microorganisms, with a minor contribution from plants growing over the cave. Despite the exhaustive qualitative analysis of organic-rich layers, the slow growth rate of these speleothems does not allow a continuous and high resolution reconstruction of past fire activity. Landscapes mantled by thin or even absent soils underlain by fractured bedrock favor the transfer of PAHs to the karst system and limit soil microbial reworking (Sun et al., 2019). The geologic and hydrologic conditions of cave KNI-51, where the thin and organic carbon-poor soils do not act as a broad carbon reservoir, and where the cave is shallow and hosted by fractured bedrock (see below), are thus well suited to the rapid transmission and preservation of discrete fire-related signals.

In order to provide a deeper understanding of the sources of hydrocarbons to cave KNI-51, the distribution of *n*-alkanes was here used in support of the PAH signal interpretation from speleothems. As one of the major components of epicuticular waxes and due to their resistance to degradation, *n*-alkanes are widely used to reconstruct vegetation shifts ascribable to climate change or land use, which affect the distribution and abundance of alkane chain lengths. Higher plants preferably synthesize long (C>25), odd carbon numbered *n*-alkanes, while shorter compounds are mainly of algal and microbial origin. Several indexes are used to assess the sources of *n*-alkanes and post-depositional processes affecting the distribution. Among these, the Carbon Preference Index (CPI) is used to evaluate the degree of odd-over-even predominance (OEP) of carbon chains (De la Rosa et al., 2012; Bush and Mclnerney, 2013) and is calculated as follows:

$$CPI = \frac{\sum_{odd} C_{21-33} + \sum_{odd} C_{23-35}}{2\sum_{even} C_{22-34}}$$

where $\Sigma_{odd}C_{21\text{-}33}$ and $\Sigma_{odd}C_{23\text{-}35}$ are, respectively, the sum of mass-normalized concentrations of odd-numbered carbon chains in the range of 21 through 33 and of 23 through 35, while $\Sigma_{even}C_{22\text{-}34}$ is the sum of mass-normalized concentrations of even-numbered carbon chains in the 22–34 range.

Fires have been shown to affect the chain length and odd–even distribution of soil *n*-alkanes. Heat drives the thermal breakdown of carbon chains, shifting the distribution towards shorter even and odd compounds. Thus, *n*-alkanes have proven useful as molecular proxies of biomass burning (Eckmeier and Wiesenberg, 2009; Kuhn et al., 2010; De la Rosa et al., 2012).

2. Methods

2.1. Study site and samples

Cave KNI-51 is located in the Kimberley region of northeast Western Australia (15.18° S, 128.37° E; ~100 m a.s.l.) (Fig. 1). This area is sparsely populated and the cave is remote, located more than 40 km from the nearest town (Kununurra; population 5,300), 25 km from the nearest paved road, and more than 1 km from the nearest unpaved (dirt) track, which experiences vehicular traffic only infrequently and which is impassable during the wet season. Electricity is produced for Kununurra and the other regional town of Wyndham via a hydroelectric plant on the Ord River, and thus potential for fossil fuel combustion to contribute anthropogenic PAHs to the cave site is minimal.

Regional climate is characterized by modest seasonal changes in temperature (mean peak daily temperatures of 36 °C in summer vs 31 °C in winter) but substantial differences in seasonal precipitation are associated with the Indo-Australian summer monsoon. Annual rainfall near KNI-51 averages ~850 mm, ~85 % of which falls in the austral summer (December-March). Bushfires are common throughout the dry season, due to human activity including both cultural and management burns, and arson and, in the late dry season (September-November), lightning strikes (Fig. 1b, 1d). In general fires in the early dry season are less intense than the late dry season because of differences in fire weather conditions and fuel moisture (Williams et al., 1998). The vegetation near KNI-51 is predominantly savanna (Fig. 2a), dominated by fire-sensitive *Eucalyptus confertiflora*, *E. foelsheana*, and *E. tectifica*, while the broader landscape includes eucalypt woodlands and mix woodlands/grasslands, with some areas of tussock grasslands that are typically burned in the second half of the dry season (July to October) (Department of the Environment and Energy, 2020; Bureau of Meteorology, 2023).

Cave KNI-51 appears extremely well-suited to the rapid transportation of organic compounds from the land surface to the underlying cave. KNI-51 is shallow (~10 m of bedrock above the roof of the stalagmite chamber) and overlain by permeable and fractured limestone. Soils are thin and poorly developed, containing little organic carbon, and limestone pavement is exposed along several portions of the land surface above the cave (Fig. 2a) including the stalagmite chamber, which is located 500 m from the single, small cave entrance. A two-year, sub-hourly environmental monitoring program in the stalagmite chamber reveals moderate seasonal swings in temperature, with temperatures during the wet season (December-March), when the majority of stalagmite growth occurs, broadly consistent from year to year (29.7

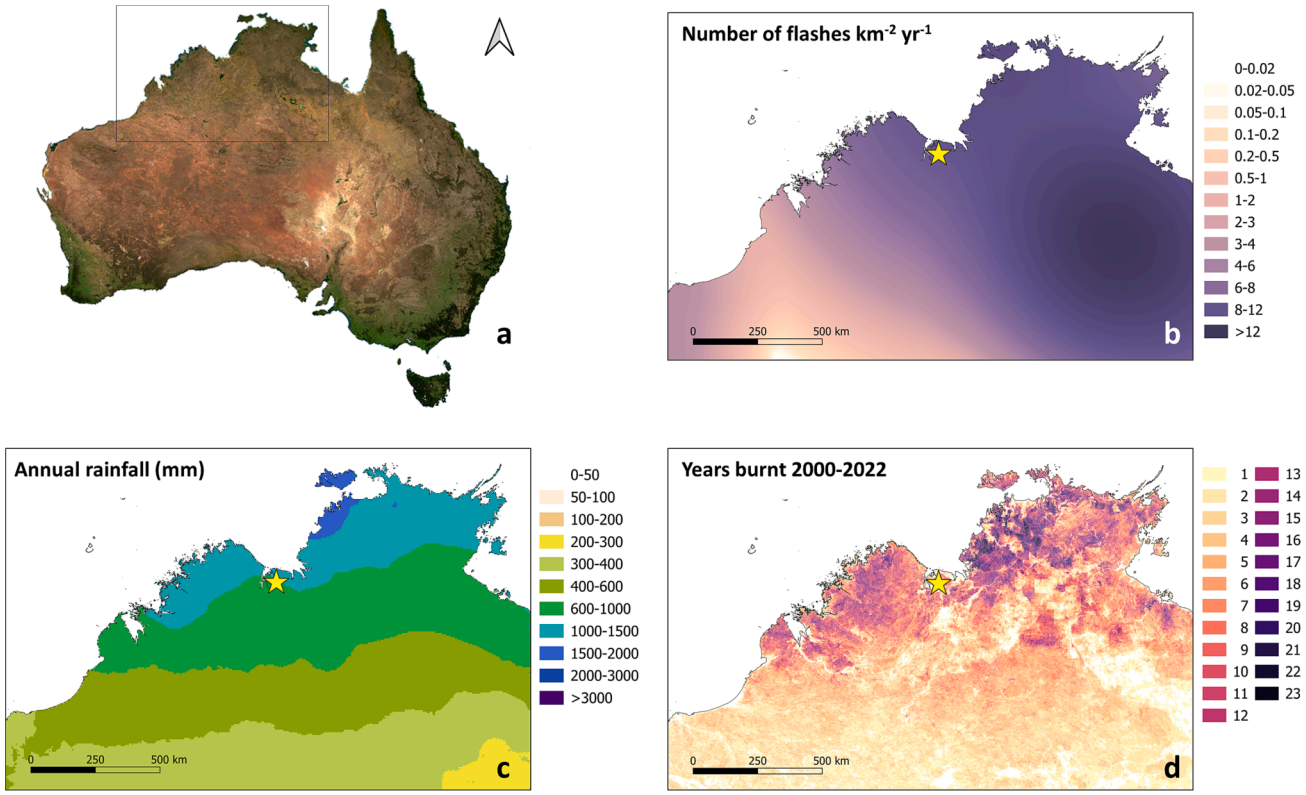

Fig. 1. (**a**) Satellite map of Australia (source: Google Maps 2021) with zoom on the Kimberley region (black rectangle). (**b**) Average annual ground lightning flash density; (**c**) annual rainfall (mm) (source of data in **b** and **c**: Australian Government Bureau of Meteorology, www.bom.gov.au). (**d**) Density map of 2000–2022 burn frequency (source: North Australian Fire Information, www.firenorth.org.au). Yellow star denotes location of cave KNI-51.

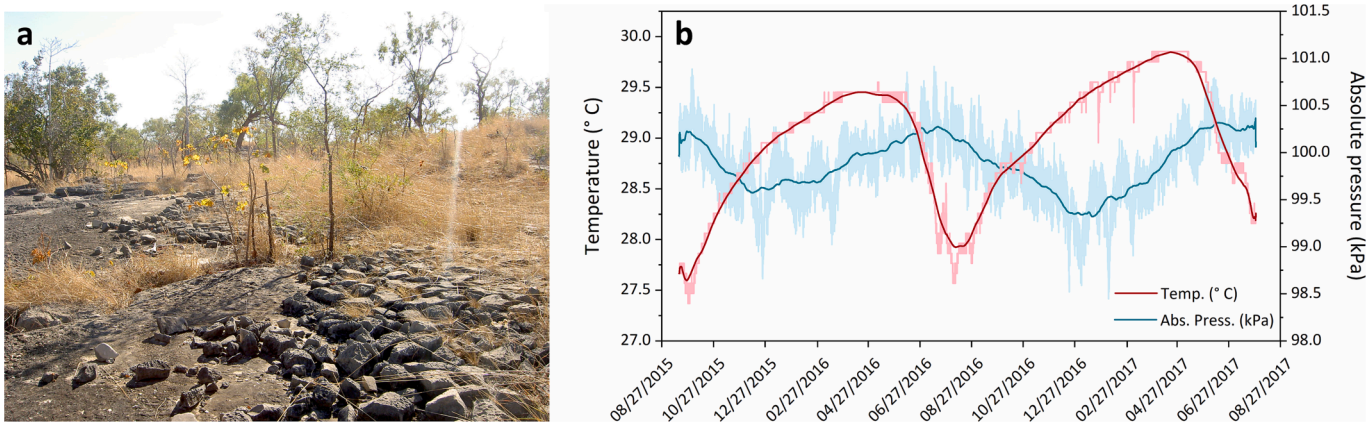

Fig. 2. (**a**) Limestone pavement, thin soil, and mixed vegetation above cave KNI-51 (photo by R. Denniston). (**b**) Sub-hourly temperature (° C) and pressure (kPa) data collected in the stalagmite chamber of cave KNI-51 (located 500 m from the entrance) from 09/16/2015 to 07/29/2017. Data collected using Onset HOBO data loggers. For clarity, spikes in barometric pressure related to flooding of the stalagmite chamber were removed.

± 0.2 °C) during the monitoring period (Fig. 2a). Barometric pressure is also seasonally variable, but air exchange is minimal (as inferred from humidity maintained at 100 % despite the absence of standing water in the cave and ambient atmospheric relative humidity averaging ~25 % during the eight month-long dry season, see Fig. S1) and thus transport of aerosols into this remote portion of the cave can be discounted.

KNI-51 stalagmites are also well-suited for this analysis. Previous dating of KNI-51 stalagmites by uranium–thorium disequilibrium methods has yielded high precision age models (2 s.d. errors of ±1–2 yr over much of the last century) and revealed fast growth (1–2 mm/yr), that together offer the possibility of high temporal resolution (Denniston et al., 2016). KNI-51 stalagmites also contain numerous sediment layers formed when the stalagmite chamber flooded and deposited clays and silts on stalagmite caps that became embedded in the matrix when flood waters receded and growth resumed (Denniston et al., 2015). These flood layers, which range in thickness from <1–10 mm, were evaluated as possible sources of PAHs as part of this study. Three KNI-51 stalagmites grew across the last millennium (see Fig. S2) - KNI-51-F (CE ~1100–1620), KNI-51-G (CE ~1320–1640), and KNI-51-11 (CE ~1750–2009) and serve as a framework for this test of paleofire activity. When collected in 2009, stalagmite KNI-51–11 was actively growing, while stalagmites KNI-51-F and KNI-51-G were collected in 2011 and were broken and lying on the cave floor.

2.2. Standards and reagents

Pesticide-grade (SpS and UpS) dichloromethane (DCM), *n*-hexane, and acetone and 34–37 % SpA hydrochloric acid (HCl) from Romil Ltd. were employed for analysis of organic compounds in KNI-51-11. Isotope-labeled standard solutions ($^{13}C_6$-acenaphthylene, $^{13}C_6$-phenanthrene, $^{13}C_4$-benzo(a)pyrene, and $^{13}C_6$-chrysene) were purchased from Cambridge Isotope Laboratories, while native PAHs were acquired from Dr. Ehrenstorfer™ (PAH Mix-9). All *n*-alkane native standards were from Sigma-Aldrich. All tools and glassware were pre-washed with a 5 % Contrad aqueous solution and rinsed three times with *n*-hexane and DCM, respectively. Where possible, glassware was also muffled at 400 °C for 4 h.

2.3. Software

Thermo Fisher Scientific Chromeleon™ 7 and Agilent MSD Chemstation E.02.00.493 were used for processing chromatograms. OriginPro 2018 was used for producing plots and for the statistical treatment of data, while maps were created with QGIS 3.18.1. Spatial analyses were conducted in R (R Core Team, 2021) using the packages 'raster' (Hijmans, 2020) and 'rgdal' (Bivand et al., 2023).

2.4. Sample preparation

2.4.1. Contamination control

As described thoroughly by Wynn and Brocks (2014) and Blyth et al. (2006), low concentrations of organic compounds in speleothems elevate the risk that chemical signals can be altered by contamination. Wynn and Brocks (2014) attributed decreasing concentrations of lipids (such as fatty acids and sterols) with distance inward from the surface of stalagmites to surface contamination. However, unlike PAHs, which are mostly regarded as atmospheric gaseous and particulate contaminants, lipids have numerous sources related to sample handling. Contamination tests were not performed for PAHs by these authors.

External contamination from petroleum-derived compounds is also an issue, particularly in regions with active oil and gas extraction operations such as exist across northeast Western Australia. In addition, sampling, sub-sampling, transport, and laboratory operations can act as sources of organic compounds (Brocks et al., 2008). Here, several precautions were used to prevent contamination. The analysis was performed on slabs cut from the center of the stalagmite, thus minimizing the contribution of contaminants migrated from the external surface. Polyethylene plastics, a major contributor of *n*-alkanes, branched hydrocarbons, and fatty acids (Brocks et al., 2008; Cheng and Yu, 2020) were never used through sampling and analysis. Solvents were only SpS and UpS grade and were previously tested repeatedly in our laboratory for organic contamination and compared with other brands. As opposed

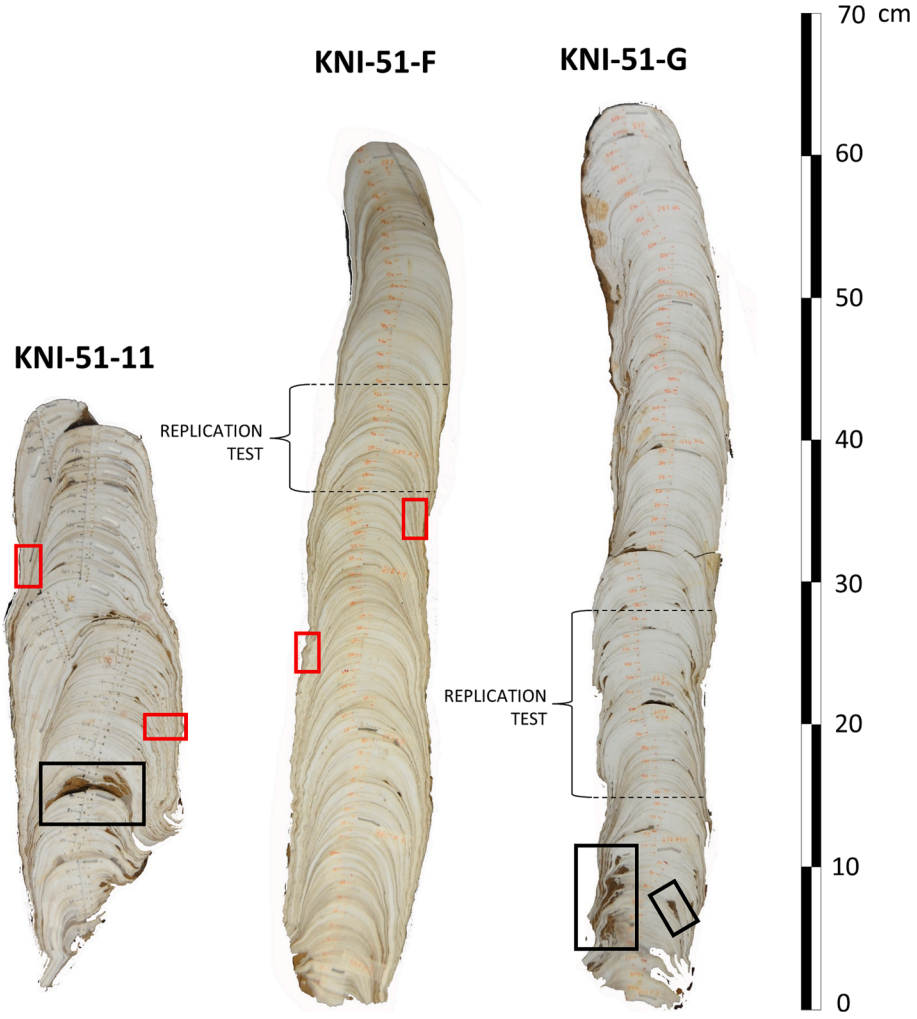

Fig. 3. Slabs of KNI-51 stalagmites. Black rectangles mark locations where flood layer sediment was extracted; red sections were used for the sequential digestion experiment; coeval sections used for the replication experiment are included between dashed lines. Distances along central growth axis of each stalagmite are faintly visible in red or black. Drill marks visible along the central axis correspond to sampling for dating and stable isotope analysis.

to previously published studies of stalagmite and rock samples, which were run under normal laboratory conditions, all samples here were treated in a class 10,000 cleanroom entirely built in stainless steel. As detailed below, rigorous blank control was also performed and possible sources of PAHs other than fire and vegetation were carefully evaluated through specific *m/z* ratios.

To test the possibility of external contamination from target compounds affecting KNI-51 stalagmites, we performed a sequential digestion test adapted from Wynn and Brocks (2014). Four rectangular sections (red rectangles in Fig. 3) averaging 10 g were cut from stalagmite KNI-51-F and KNI-51-11 residual material using a Dremel tool equipped with a cutting diamond wheel. In the organic cleanroom, the sections were cleaned in the sonic bath with *n*-hexane and dichloromethane, dried, and weighed. Sections were digested for 2 min in 20 mL of a 3 M HCl solution (pre-cleaned three times by liquid–liquid extraction with dichloromethane) to remove only an external layer averaging 1.5 g from the sections (details on sample weight are reported in Table S3). The process was repeated three times for each section to assess the distribution of organic proxies from the surface to the interior of the slabs. The residual aragonite from the interior was treated as described below for stalagmite samples, except that they were not drilled.

2.4.2. Stalagmite samples

Stalagmites KNI-51-F, KNI-51-G, and KNI-51-11 were bisected using a water-cooled trim saw and then a slab was cut from one half using a hand-held wire saw; no oils or solvents were applied to the stalagmites during cutting. Samples analyzed for PAH and *n*-alkane abundances were drilled using a Dremel handheld drill with a 1 mm diameter diamond-coated bit in order to obtain continuous samples in 2–3 mm intervals, which provides a resolution of 2 ± 1 years per sample. Prior to drilling each sample, the outer surface of the slabs was thoroughly rinsed with pesticide grade *n*-hexane and dichloromethane to guarantee the absence of contaminants. Powders were then transferred to a class 10,000 cleanroom for organic analyses and extracted. The extraction procedure is detailed in Argiriadis et al. (2019), although with slight modifications. Briefly, samples were spiked with 50 μL of the internal standard solution containing $^{13}C_6$-acenaphthylene, $^{13}C_6$-phenanthrene, $^{13}C_4$-benzo(*a*)pyrene at 1 ng μL^{-11} and with 50 μL of an hexatriacontane solution at 50 ng μL^{-1}. Then, they were dissolved in 3 M HCl and liquid–liquid extracted three times with 10 mL of DCM and 5 mL of *n*-hexane. Extracts were buffered with anhydrous sodium sulfate, reduced to ~ 200 μL under a gentle stream of nitrogen, spiked with 20 μL of $^{13}C_6$-chrysene at 1 ng μL^{-1} as a recovery standard, and analyzed by gas chromatography-mass spectrometry (GC–MS). Following the same procedure, several procedural blanks (one for every set of five samples) were processed together with samples in order to assess background contamination, which was controlled by careful cleaning and cleanroom processing, allowing the quantification of trace abundances in these samples.

2.4.3. Analysis of soil, cave sediment, and stalagmite flood sediment

Material milled from KNI-51 stalagmites is predominantly aragonite but some samples also contain flood-derived sediment. In order to investigate the contribution of these sediments to the measured distributions and abundances of PAHs, we collected and analyzed soil samples from outside the cave (D_T, D_B, and E), sediment from the cave floor (A_T, A_B, B_T, B_M, B_B, C_T, and C_B) (see Table S1), and from particularly thick flood layers contained within the stalagmites (black rectangles in Fig. 3). Three flood sediment samples were milled from stalagmites KNI-51-11 and KNI-51-G (as is visible in Fig. 3, KNI-51-F did not contain thick flood layers). The sediment samples interlayered within the stalagmites were carefully removed from the stalagmite slab with the hand drill. Soil/sediment samples, previously stored in aluminum foil pouches, were freeze-dried and then ground in a hand mortar. All samples and blanks were dispersed with diatomaceous earth, spiked with internal standards, and extracted three times (static: 5 min) through an ASE 350 (Dionex Thermo Fisher) accelerated solvent extractor using a 1:1 (*v/v*) mixture of DCM and *n*-hexane at 100 °C and 1000 psi in 22 mL stainless steel cells. Extracts were concentrated to ~200 μL under a gentle stream of nitrogen and analyzed by GC–MS.

2.5. Elemental analysis

The total carbon and total organic carbon contents in sediment and soil samples were assessed through elemental analysis (Flash 2000 Elemental Analyzer, Thermo Fisher Scientific). Dry and homogenized samples were weighed in tin capsules (~200–500 μg), combusted at 950 °C, and oxidized in a quartz reactor packed with granular silvered cobaltous/ic oxide, reduced copper, and chromium oxide in the presence of oxygen. Helium was used as a carrier gas. The instrument linear response was verified through standard acetanilide (Thermo Fisher Scientific), which allowed instrument calibration. Prior to analysis, samples for the measurement of organic carbon were treated with a 10 % HCl solution, washed, and dried. Analyses were repeated three times for each sample and results were averaged.

2.6. GC–MS and GC–MS/MS analysis

PAHs were quantified through gas chromatography coupled with triple quadrupole mass spectrometry (Thermo Scientific Trace 1310 - TSQ 9000 GC–MS/MS system). The GC was equipped with a HP-5 ms capillary column (60 m, 0.25 mm i.d., 0.25 μm film thickness, Agilent Technologies) and the temperature program was as follows: 70 °C (2 min), 10 °C min^{-1} to 200 °C (5 min), 8 °C min^{-1} to 280 °C (5 min), 5 °C min^{-1} to 310 °C (9 min). Helium was used as carrier gas (1 mL min^{-1}), while argon was used as collision cell gas. The PTV injector was operated in splitless mode (70 °C to 320 °C at 14.5 °C s^{-1}). Detailed information on *m/z* ratios, transitions, and collision energy used for single PAH compound identification are reported in Table S2.

The quantification of *n*-alkanes was performed by gas chromatography (Agilent Technologies 7890A GC) coupled to single quadrupole mass spectrometry (Agilent Technologies 5975C MS) operated in selected ion monitoring (SIM) mode (*m/z* 71, 99, 85, 113). Separation was achieved on a 60 m HP-5 ms column as follows: 50 °C (5 min), 18 °C min^{-1} to 315 °C (13 min), postrun 315 °C (15 min). Helium was used as carrier gas (1.2 mL min^{-1} flow). The inlet and transfer line temperature was 300 °C. Injection was performed in splitless mode.

Samples were analyzed also in full scan mode to evaluate the presence of non-fire related hydrocarbons and other organic compounds.

Analytes were quantified through the isotope dilution technique and results were corrected by the average response factor obtained by repeated injections, together with samples, of a solution containing all native, internal and recovery standard compounds at the same concentration (100 pg μL^{-1}). Absolute amounts were corrected by the average blank and divided by the sample weight to obtain concentration values in ng g^{-1}.

2.7. Spatial analyses

In order to evaluate the association between the detected concentrations of PAHs and the presence of fire scars in proximity of KNI-51, we compared satellite imagery of burn scars to the PAH record from KNI-51-11, which was actively growing when collected in 2009. Fire history data for the study area was obtained from Northern Australia and Rangelands Fire Information (NAFI; https://firenorth.org.au/nafi3/), which provides information on date of ignition and fire extent at a resolution of 250 m for fires since 2000. Our analysis was thus temporally restricted between the year 2000 and 2009. To improve resolution, we created fire severity maps by calculating the Normalized Burn Ratio (NBR), a spectral index which has been shown to provide reliable estimates of fire severity in savannas (e.g., Smith et al., 2007; Philipp and

Levick, 2020). NBR relies on the low absorbance and high transmittance of vegetation at near-infrared (NIR) wavelengths and its high absorbance and low transmittance at shortwave-infrared (SWIR) wavelengths (Alcaras et al., 2022), and is calculated as:

$$NBR = \frac{NIR - SWIR}{NIR + SWIR}$$

We gathered cloudless satellite imagery from Landsat 7 ETM and Landsat 8 OLI/TIRS missions (30 m resolution) captured before and after each fire that occurred within 5 km of KNI-51 since 2000, using the ignition dates provided by NAFI as a reference point. The variation in NBR (dNBR) is the difference between pre- and post-fire NBR. To maximize the accuracy of these analyses, we ensured that pre- and post-fire imagery was captured as close as possible to the ignition date (Holden et al., 2005). In the absence of field data to calibrate fire severity, we used the general thresholds proposed by the European Forest Fire Information System (EFFIS; https://effis.jrc.ec.europa.eu/about-effis/technical-background/rapid-damage-assessment) to classify pixels of each dNBR map as either unburnt, low severity, moderate severity, or high severity. For each fire severity map, we combined all pixels classified as burnt, regardless of severity. We then quantified the proportion of land burnt within buffers of different sizes, all centered on KNI-51: 50 m, 100 m, 250 m, 500 m, 1 km, 1.5 km, 2 km, 2.5 km, 3 km, and 5 km. We evaluated the association between the proportion of burnt land and the sum of LMW and MMW PAHs for each buffer using linear and quadratic regression. The best model was identified by comparing their AICc value, which is analogous of Akaike Information Criterion (AIC) corrected for small sample size, and selecting the model with the lowest AICc score (Burnham and Anderson, 2002). Analyses were conducted using the packages 'MuMIn' (Bartoń, 2023) and tidyverse (Wickham et al., 2019) in R (R Core Team, 2023).

3. Results

3.1. Sequential digestion

To the best of our knowledge, no PAH data from sequential digestion of stalagmites have previously been published and thus the following represents the first test of external contamination on stalagmite PAH values. Results are reported in the research data. Here, no clear decreasing trend in concentrations of PAHs towards the interior of the stalagmite is observed. In fact, concentrations tend to be similar, or even more elevated in the interior layers than across the exterior in most samples. The boxplots in Fig. 4 evidence the absence of any trend or significant differences among layers, implying that variations in the concentrations found in progressive layers are due to fluctuations around the mean rather than the result of external contamination.

3.2. PAHs in KNI-51 soil, cave sediment, and stalagmite flood sediment

Since most hydrophobic organic compounds are generally strongly bound to organic matter in sediments and particulates (Pignatello,

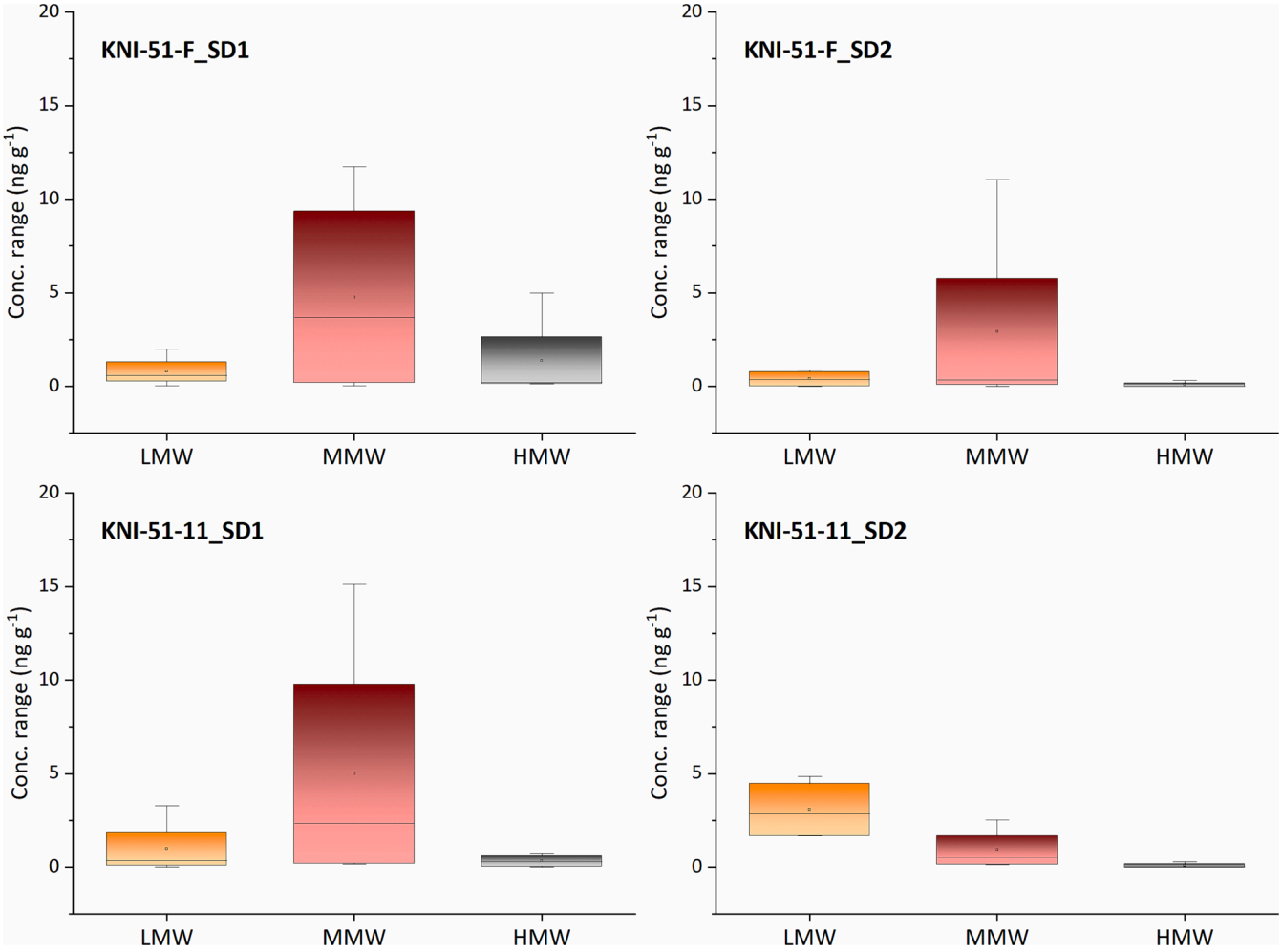

Fig. 4. Inter-layer concentration variations of LMW, MMW, and HMW PAHs in the four stalagmite sections (top: KNI-51-F; bottom: KNI-51-11) used for the sequential digestion experiment.

1998), sediments included as flood layers in stalagmites might represent an additional source of organic compounds and thus could affect the suitability of stalagmites as archives of organic paleofire proxy data. For this reason, we evaluated the presence of PAHs in the cave sediment and in thick flood layers contained in stalagmites from cave KNI-51.

The distribution of target compounds in soils from inside and outside the cave was used to assess their possible contribution to stalagmites. Highest total PAH concentrations were measured in soil samples from outside the cave (samples D_T, D_B and E, Fig. 5b), with the highest contribution from HMW compounds, namely benzo(*a*)pyrene and benzo (*e*)pyrene (Figs. 5 and 6). Sample E, collected farthest from (~20 m) and above the cave entrance, was the only sample where indeno(1,2,3-*cd*) pyrene was above the limit of detection. Naphthalene was the only compound present in all ten samples, while acenaphthylene, perylene, benzo(*ghi*)perylene and dibenzo(*ah*)anthracene were always below the detection limit. Total PAH concentrations in samples from within the cave (samples A to C) are dominated by naphthalene, chrysene and benzo(a)pyrene. Naphthalene and phenanthrene are the dominant compounds in stalagmite thick flood layer sediment samples (KNI-G a, KNI-G b, KNI-11, Fig. 5a), followed by acenaphthylene. Compared to soil and sediment samples, the concentration of LMW PAHs in stalagmite flood sediments is high mainly due to elevated levels of naphthalene in all three samples. Among HMW PAHs, perylene, benzo(*ghi*)perylene, dibenzo(*ah*)anthracene, and indeno(1,2,3-*cd*)pyrene were not detected, while benzo(*e*)pyrene was the only 5-ring compound present in all three samples. The sample from stalagmite KNI-51–11 contained the highest number of compounds and was the only one where fluoranthene, pyrene, benzo(*b*)fluoranthene and benzo(*k*)fluoranthene were present. In summary, we observe a similar PAH composition in soil, sediment, and stalagmite flood sediment, although the latter presents higher concentrations of compounds, as summarized in Figs. 5 and 7.

Given that organic carbon can serve as a reservoir for adsorbed PAHs, we also measured TOC in these sediment samples. TOC varies between 2 and 5 % by weight (see Table S4), but this variation does not appear to affect concentrations of organic compounds, which were therefore not normalized to TOC. Indeed, no significant correlation (Pearson) was found between total PAHs and TOC ($r = 0.24$, p-value = 0.51). These values of TOC are in line with global means for tropical and subtropical grasslands, savannas, and shrublands (Stockmann et al., 2015), and with values reported for red earths in fire-prone tropical northern Australia (Chen et al., 2005).

3.3. PAH in stalagmite aragonite

The entirety of two of the three stalagmites (KNI-51-F and KNI-51–11) were processed and were thus compared in terms of concentration levels and distribution of PAH compounds. Results from KNI-51-G are not included in this analysis since only a section of it was processed for the replication test. Although samples were processed as time-series, results will be shown and discussed here only in a geochemical perspective in order to fulfil the scope of this paper, that is to test the validity of PAHs as fire tracers in speleothems and provide a framework for future interpretation in a paleoenvironmental context. Although generally present in trace concentrations (sub-ng to ng level), PAHs were detected in 182 of the 192 (95 %) samples milled from KNI-51-F and in 206 of 208 (99 %) from KNI-51–11. Total PAH concentrations (ng/g) range from below the level of detection to 32 ng g^{-1} in KNI-51-F and to 60 ng g^{-1} in KNI-51-11.

The MMW phenanthrene has the highest average concentration in KNI-51-F (0.7 ng g^{-1}; Fig. 6), followed by the LMW naphthalene (0.5 ng g^{-1}) and the HMW benzo(*a*)pyrene (0.4 ng g^{-1}); the HMW perylene has the lowest average concentration (0.01 ng g^{-1}). LMW and MMW PAHs are most common: MMW PAHs pyrene (65 % of samples), phenanthrene (52 %), fluoranthene (46 %), retene (45 %) followed by LMW PAHs: naphthalene (55 %) and fluorene (40 %) (Fig. 7). All other PAH compounds are present in fewer than half of the samples. LMW and MMW compounds therefore dominate the distribution, although some significant spikes of benzo(*a*)pyrene are present up to a maximum concentration of 14 ng g^{-1}, accompanied by other HMW compounds such as benzo(*e*)pyrene (7 ng g^{-1}) and benzo(*ghi*)perylene (10 ng g^{-1}). As a result, average concentrations of total HMW PAHs in KNI-51-F are comparable with mean total LMW (0.9 and 1.0 ng g^{-1}, respectively).

HMW mean PAH concentration in stalagmite KNI-51–11 are significantly lower (0.1 ng g^{-1}) than in KNI-51-F, while mean LMW and MMW average 1.4 and 2.0 ng g^{-1}, respectively. Naphthalene has the highest mean value (1.1 ng g^{-1}) - although it is present only in 11 % of the samples – followed by pyrene (0.6 ng g^{-1}) and phenanthrene (0.6 ng g^{-1}). Pyrene is the most common compound in KNI-51–11 (96 % of samples), followed by fluoranthene (69 %) and phenanthrene (57 %), as shown in Fig. 6. MMW PAHs dominate in KNI-51–11 as in KNI-51-F, although in the latter the three classes of PAHs are distributed as follows: LMW 28 %, MMW: 45 %, HMW 27 %, while in KNI-51–11 the composition is: LMW 40 %, MMW 56 %, HMW 4 %. Fig. 6 summarizes the mean distribution of PAHs in the two stalagmites.

Full scan sample chromatograms reported in the Supplementary

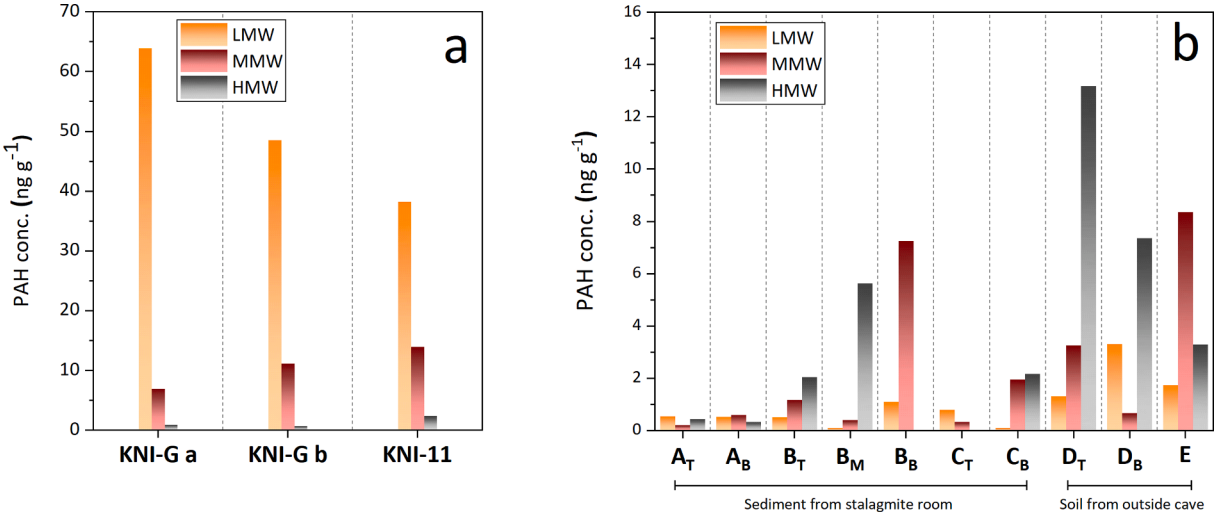

Fig. 5. Concentrations (ng g^{-1}) of low (LMW, orange), medium (MMW, red), and high (HMW, grey) molecular weight PAHs (a, b) in flood layer sediments from stalagmites KNI-51-G and KNI-51-11 (a) and in soil/sediment samples from inside and outside the cave (b).

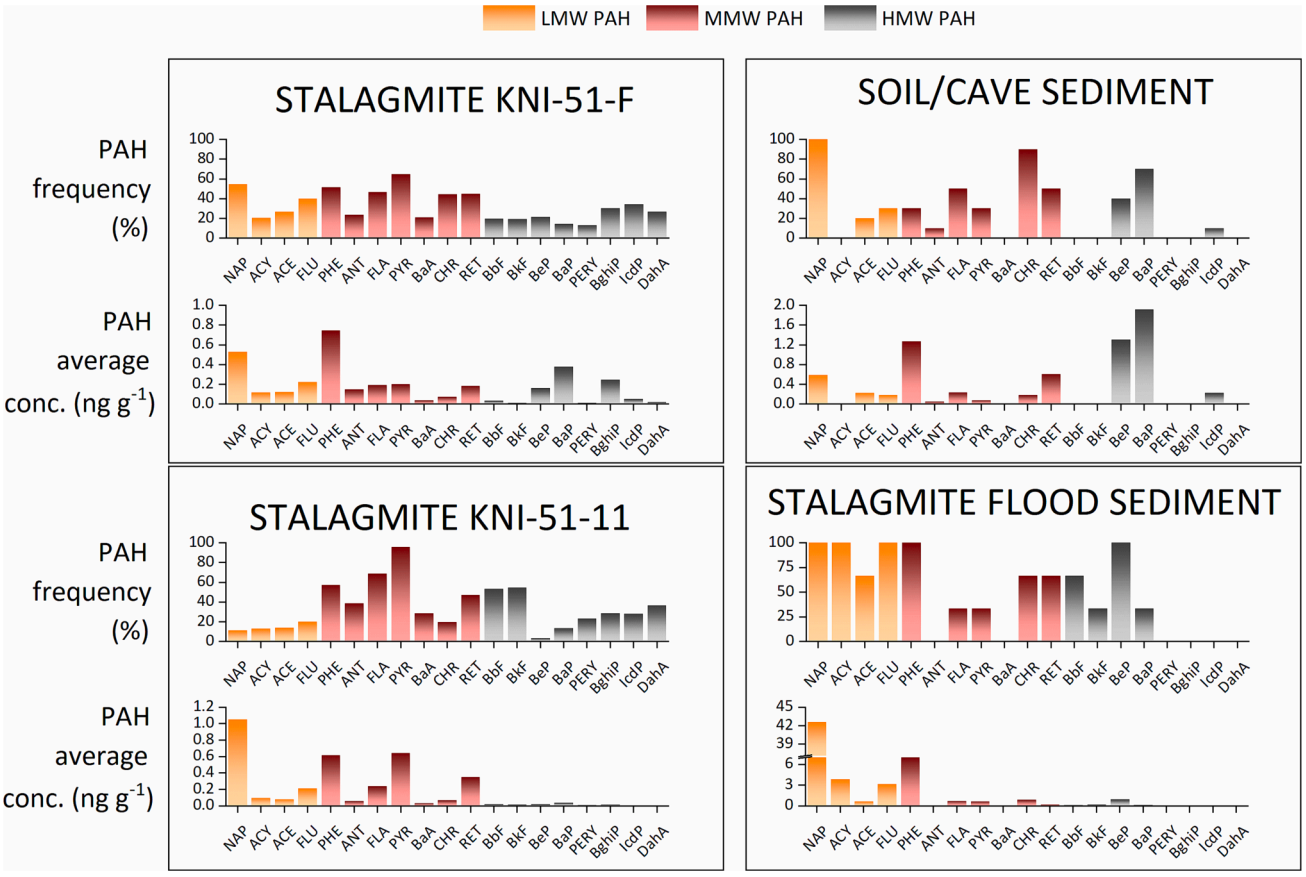

Fig. 6. Frequency (% of samples where each compound was above the limit of detection) and average concentration (ng g^{-1}) of PAHs in stalagmite KNI-51-F, KNI-51-11, soil/cave sediment and stalagmite flood sediment.

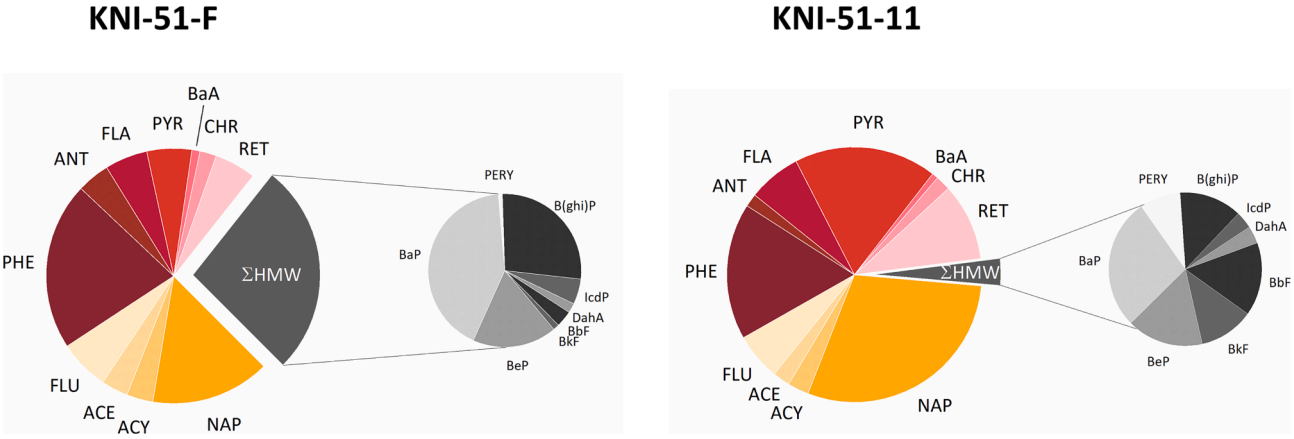

Fig. 7. Mean distribution of PAHs in aragonite samples from stalagmites KNI-51-F (left) and KNI-51-11 (right). Orange: LMW PAHs, red: MMWs, grey: HMWs.

Material together with *m/z* 128 + 142 + 156 and 178 + 192 + 206 (Figs. S3-S5, Fig. S6) show no significant presence of methylated PAH compounds often found in presence of petroleum sources. The majority of peaks present in the full scan chromatograms are ascribed by NIST library search to biogenic volatile organic compounds associated to plants, bacteria, and fungi, such as terpenes, carboxylic acids, aliphatic ketones and aldehydes, fatty acids, and phenolic compounds. Among others, we identified phenol and benzoic acid derivatives, long chain fatty aldehydes and ketones and anthraquinones, that are often detected in plant extracts and were found to exert diverse antimicrobial activities. In addition, the classes of compounds found in full scan chromatograms have been shown to be widely present also in smoke and particulates from biomass burning.

3.4. Linear alkane distribution

The distribution of *n*-alkanes was assessed in all samples to further investigate the sources of hydrocarbons to the cave. Data for soil and sediment are shown in Fig. S7 and research data. All compounds in the C_{13}-C_{34} range were present in soil samples. Total *n*-alkane concentrations were significantly higher in thick mud layers (12–24 μg g^{-1}) than in soil (0.3–2.4 μg g^{-1}), equally distributed between odd and even

compounds. With respect to the Carbon Preference Index (CPI), stalagmite thick flood layers average near 1 (0.95–1.26), while most cave sediment and soil samples are below 1 except for samples A_B (1.31) and B_B (2.74). Thus, no OEP was observed in these samples.

Out of 10 sediment and soil samples, C_{15} (*n*-pentadecane) and C_{17} (*n*-heptadecane) were present in 8 and 9, respectively, and were significantly higher (C_{15}: 57–803 ng g-1; C_{17}: 15–917 ng g^{-1}) than other short-chain *n*-alkanes; flood layer sediments were particularly rich in these two compounds (C_{15}: 0.2–2 μg g^{-1}; C_{17}: 0.3–0.4 μg g^{-1}). In general, thick mud layers are approximately one order of magnitude richer in the *n*-alkane content than soil and sediment samples.

Single *n*-alkane concentrations measured in stalagmite KNI-51-F range from below the limit of detection to 1.7 μg g^{-1} (C_{28}). The most frequently detected compounds fall in the C_{23}-C_{32} range (Fig. 8), with C_{21}, C_{23}-C_{27}, C_{29}-C_{34} being detected in more than 80 % of the samples. Mean and maximum concentrations follow a normal distribution centered at C_{28} (mean: 162 ng g^{-1}), with the exception of C_{15}, which is, on average, slightly more abundant than other short chain compounds, as was observed also in flood layers, cave sediments, and soil samples. The distribution of compounds in the C_{21}-C_{35} interval in stalagmite KNI-51–11 is similar to KNI-51-F. However, mean concentrations are higher for short compounds in the C_{10}-C_{17} range compared to long carbon chains in KNI-51–11, resulting in a multi-modal distribution with maxima at C_{11} (347 ng g^{-1}), C_{17} (289 ng g^{-1}), and C_{29} (205 ng g^{-1}).

Similar to sediment, soil, and mud layer samples, no marked OEP was observed in KNI-51-F: CPI values range from 0.3 to 7 (average 1.1 ± 0.7), although only one-third of the samples have a CPI greater than 1. In KNI-51–11, the CPI is more variable, with values in the 0.06–13 range (average 1.4 ± 1.7), of which 56 % is greater than 1. The ACL in KNI-51–11 ranges 12–28 with an average value of 20 ± 4.

Sample chromatograms from *m/z* 85 are reported in the Supplementary Material (fig. S2). Despite the lack of OEP, the presence of the pristane and phytane characteristic peaks, typically recognized as a petroleum signature, was not revealed.

3.5. Correlation analysis

The relationship between PAHs in flood layers and stalagmite carbonate was investigated through correlation analysis. The presence of flood layers in the two stalagmites, reported by Denniston et al. (2015) as binary data (0 = absent, 1 = present), was correlated with the presence of PAHs. First, all data were interpolated at 0.5 mm to be equally spaced and smoothed (5 pts adjacent average). Then, the Pearson correlation and p-value were computed for flood data and organic compounds. Correlations were tested for single compounds and groups (total PAH, LMW, MMW, and HMW PAH).

All correlation results are reported in the research data, and correlations of single compounds are shown in Fig. 9. The significance test at the $\alpha = 0.05$ level shows all computed correlations between the presence of PAHs and the occurrence of mud-rich layers in the stalagmites are statistically significant. Correlations between PAH groups (LMW, MMW, HMW, Total) and flood layers are generally low and positive and similar for the two stalagmites (0.09–0.16 in KNI-51–11 and −0.06–0.10 in KNI-51-F), as indicated by correlation coefficients and p-values. PAH groups are well correlated with each other and with total PAHs with moderate to high positive values (>0.5) in both stalagmites although in KNI-51-F the correlation of LMW PAH with MMW, HMW, and total PAHs is lower (0.13–0.44). The correlations of single PAH compounds with the presence of flood layers are negligible (r = -0.06 to 0.16 in KNI-51-F and −0.07 to 0.24 in KNI-51–11), with highest values detected for select 5- and 6-ring (HMW) PAHs, namely benzo(*b*)fluoranthene, benzo(*k*)fluoranthene, benzo(*a*)pyrene, benzo(*ghi*)perylene, and indeno(1,2,3-*cd*)pyrene.

3.6. Proxy replication in different stalagmites

Waters migrating from the land surface to a cave follow a myriad of pathways, each with its own set of physicochemical characteristics that can distort or mask fluid geochemistry. As a result, different cave drip waters, and thus the stalagmites they produce, can have different geochemical compositions (Duan et al., 2016). A robust test for the presence of secondary effects involves the analysis of two or more coeval stalagmites. If samples formed at the same time exhibit similar geochemical trends, then it is likely that these represent a spatially significant environmental signal (such as bushfire) that was not meaningfully impacted by processes occurring in the bedrock. Thus, in order to test the replication of PAH abundances and distributions between different stalagmites, a 135 mm subsection of KNI-51-G (see Fig. 3) was drilled and analyzed to be compared with a coeval section of KNI-51-F. Differences in stalagmite growth rates resulted in lower temporal resolution in KNI-51-F (1.15 mm yr^{-1}; ~2–3 yr resolution) than in KNI-51-G (1.99 mm yr^{-1}; ~1 yr resolution). Concentrations (Fig. 10) in both

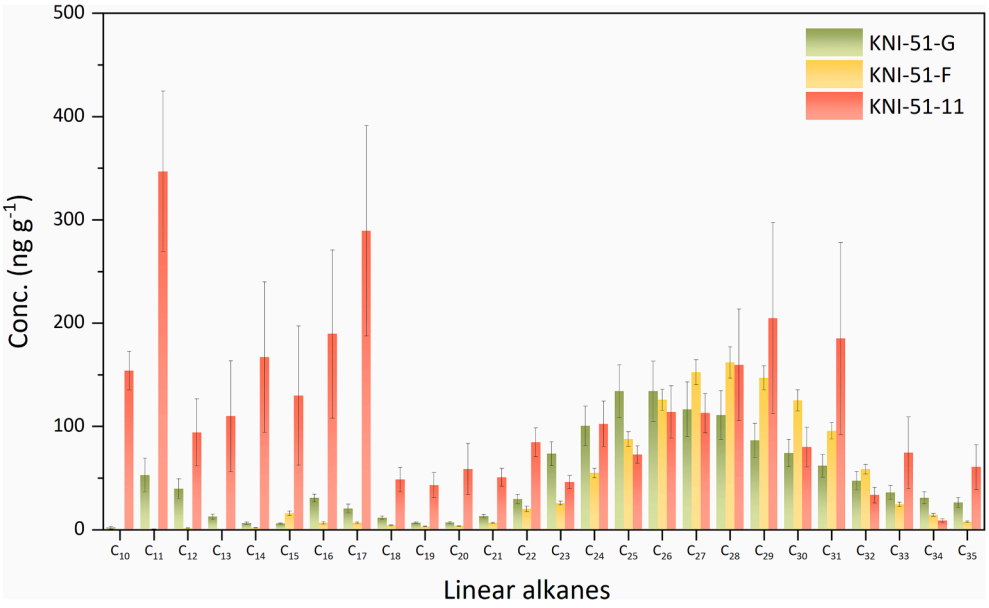

Fig. 8. Mean distribution and standard error of *n*-alkanes in stalagmites KNI-51-F, KNI-51-G and KNI-51-11.

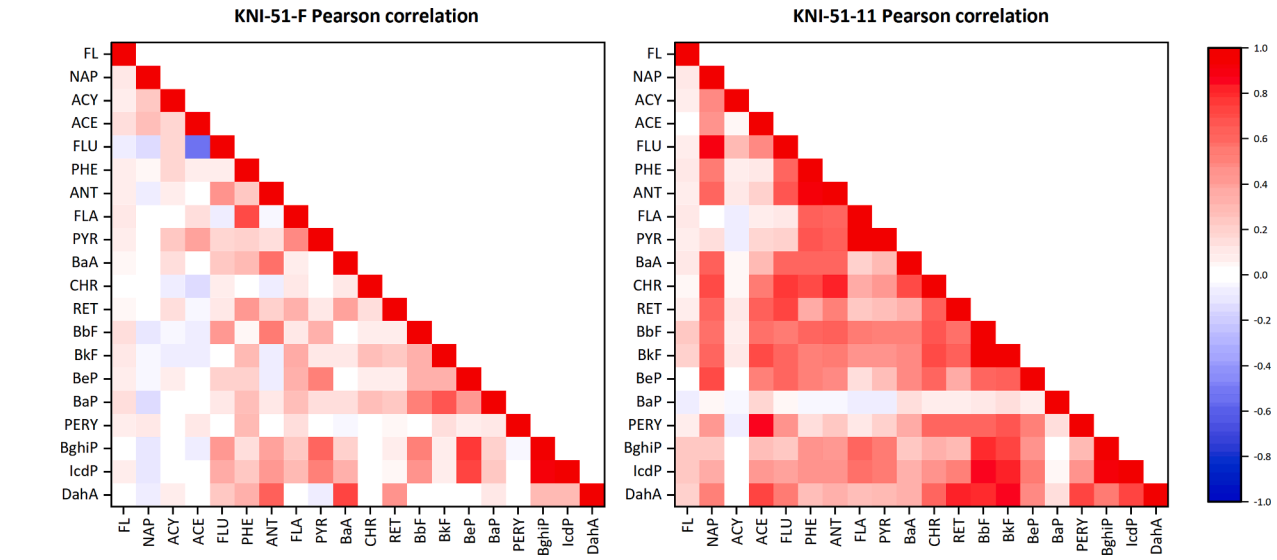

Fig. 9. Pearson correlation of single PAH compounds with flood layers (FL) in stalagmites KNI-51-F (left) and KNI-51-11 (right).

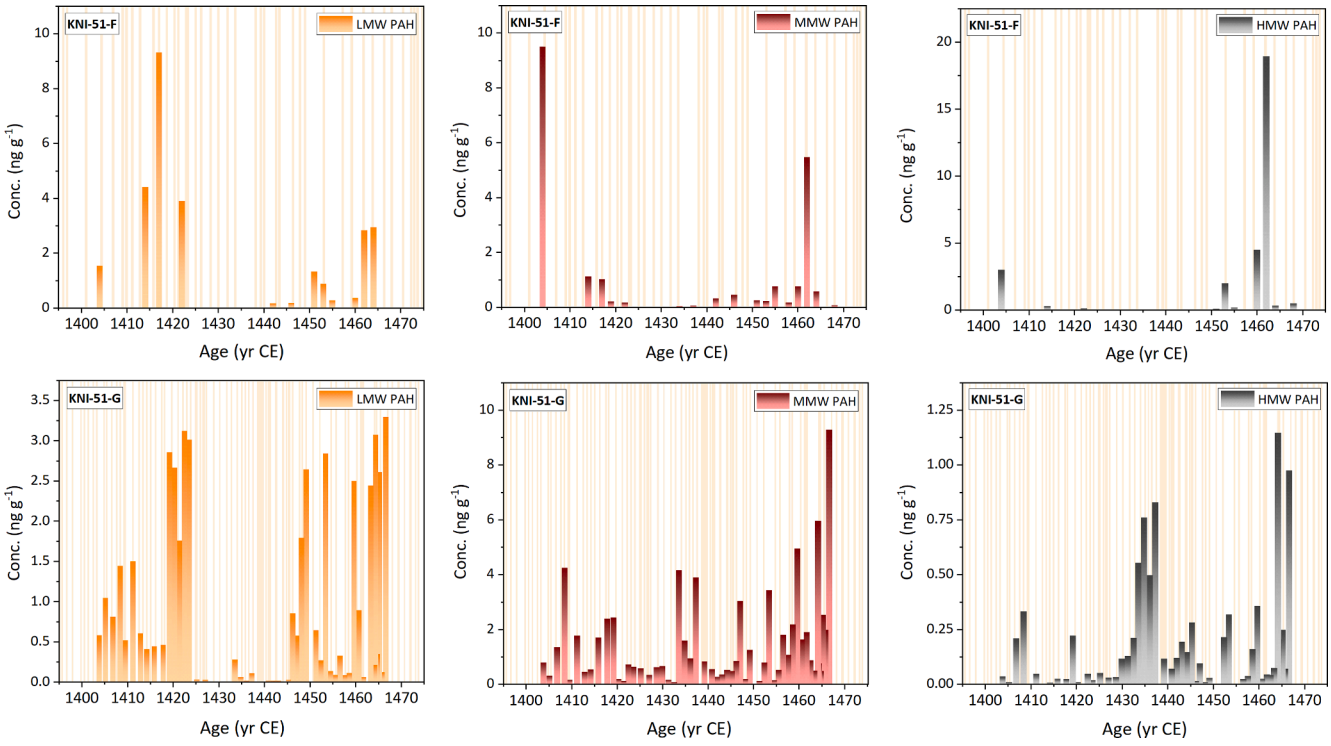

Fig. 10. PAH concentrations (orange: LMW, red: MMW, grey: HMW) in two coeval sections of stalagmite KNI-51-F (top) and KNI-51-G (bottom). Beige bars in the background represent flood layers in the stalagmites.

stalagmites are in the ng to sub-ng/g range, with slightly lower values in KNI-51-G. Peaks in all three weight classes of PAHs are visible in both stalagmites at 1400–1420 and 1450–1460 CE. When factoring in age model uncertainties, the replication of LMW PAHs is particularly robust. However, spikes in MMW and HMW PAHs in the period 1430–1440 CE apparent in KNI-51-G are not present in KNI-51-F.

Because the infiltration network above a cave can be complicated, each drip can have its own distinct set of characteristics, and thus the replication of geochemical values and trends in coeval stalagmites represents an important test of the veracity of the inferred paleoenvironmental signal (Dorale and Liu, 2009). Based on our analysis, PAH generally show broad agreement between two different KNI-51 stalagmites for the period 1380–1480 CE, including all molecular weights below detection from 1380 to 1400 and 1470–1480 CE in both stalagmites and peaks at ~1405–1420 and 1450–1465 CE. Overall, these results support their ability to capture and conserve the paleofire signal, although elevated concentrations of HMW PAHs in KNI-51-G at ~1435 CE are not present in KNI-51-F. It is unclear if this discrepancy is due to differential flow regimes (i.e., matrix vs. fracture flow) through the overlying bedrock. The overall similar trends in different molecular weight PAHs between stalagmites KNI-51-F and KNI-51-G suggest that these are primary paleoenvironmental signals, unaffected by other processes occurring in the overlying soil or bedrock.

3.7. Association with fire scars

In order to provide a more nuanced view of fire activity, we relied on dNBR rather than fire scars (Fig. 11a). Moderate-severity fires were detected only when evaluating fire severity within 1.5 to 5 km of KNI-51, and never accounted for more than 1.2 % of the area, with the remaining fires all being of low severity (Table S5 in Supplementary Material). We identified an association between the proportion of burned land and the combined LMW and MMW PAH concentrations in stalagmite KNI-51–11 only when investigating buffers with radii of 2–5 km from the cave (Fig. S8). The best model, selected based on AICc scores, was based on a quadratic regression using a 5-km buffer (adjusted-R2 = 0.97, p value = 2.4×10^{-6}; Fig. 11-bc). Although the predominance of low-severity fire made it impossible to explore the variation in PAH concentration associated with fire severity, the increase in PAH concentration was particularly evident when the proportion of land burnt exceeded 60 % of the examined area within 2–5 km from the cave (Fig. 11b, Fig. S8).

4. Discussion

4.1. Evaluation of external contamination sources

Although the discontinuity of the stalagmite structure affects the homogeneity of the acid digestion process, creating areas where the dissolution occurs at different rates according to small-scale heterogeneity in hardness and solubility, the sequential digestion test demonstrated that external contamination does not appear to be a source of PAHs on these stalagmites since concentrations are not correlated with distance from the sample margin. Despite variations likely related to the aforementioned inhomogeneity of the structure, results do not differ significantly between each other, as shown in the boxplots in Fig. 4, and all are consistent with results obtained on the stalagmite samples despite differences in the extraction technique. Therefore, we conclude that PAH distributions are not derived from collection, transport, and subsampling operations.

4.2. Possible roles of non-fire related sources

n-Alkanes in KNI-51 soil, sediment, and stalagmite aragonite consistently lack the OEP commonly detected in soils and sediments (Castañeda and Schouten, 2011) and attributed to the tendency of terrestrial plants to synthesize odd-numbered carbon chains. This occurrence is rarely reported in environmental records and thus we dedicated this additional paragraph to possible interpretations. In consideration of the lack of OEP observed in most samples analyzed and owing to the proximity of the cave to regional oil wells, we investigated the possibility that hydrocarbons from petroleum deposits were responsible for the observed stalagmite PAHs. Other possible sources of hydrocarbons are discussed as well. Cave KNI-51 is proximal to the southernmost boundary of the Milligans-Kuriyippi/Milligans petroleum system, one of the sub-systems of the Bonaparte basin, a mainly offshore petroleum basin with a few abandoned onshore wells drilled between 1972 and 2001 CE and used for exploratory purposes. The basin is considered promising especially for offshore gas extraction, while only limited liquid hydrocarbon reservoirs were discovered so far. Six wells, 700–2553 m deep, are present within 20 km east of the cave position, none of which are currently working. However, gas discovery is reported for all these wells with small oil shows, likely representing local generation from basinal shale facies, at *Waggon Creek 1* and *1A* and *Ningbing 2*, located 10 and 11 km from the cave, respectively. Conversely, oil discovery is limited to few offshore sites (Earl, 2004; Ahmad and Munson, 2012; Geoscience Australia, 2021).

Cave KNI-51 is part of the Late Devonian limestone sedimentary geological unit named the *Ningbing Group*, which is overlain by the Carboniferous sandstone *Milligans Formation*, which in turn is believed to

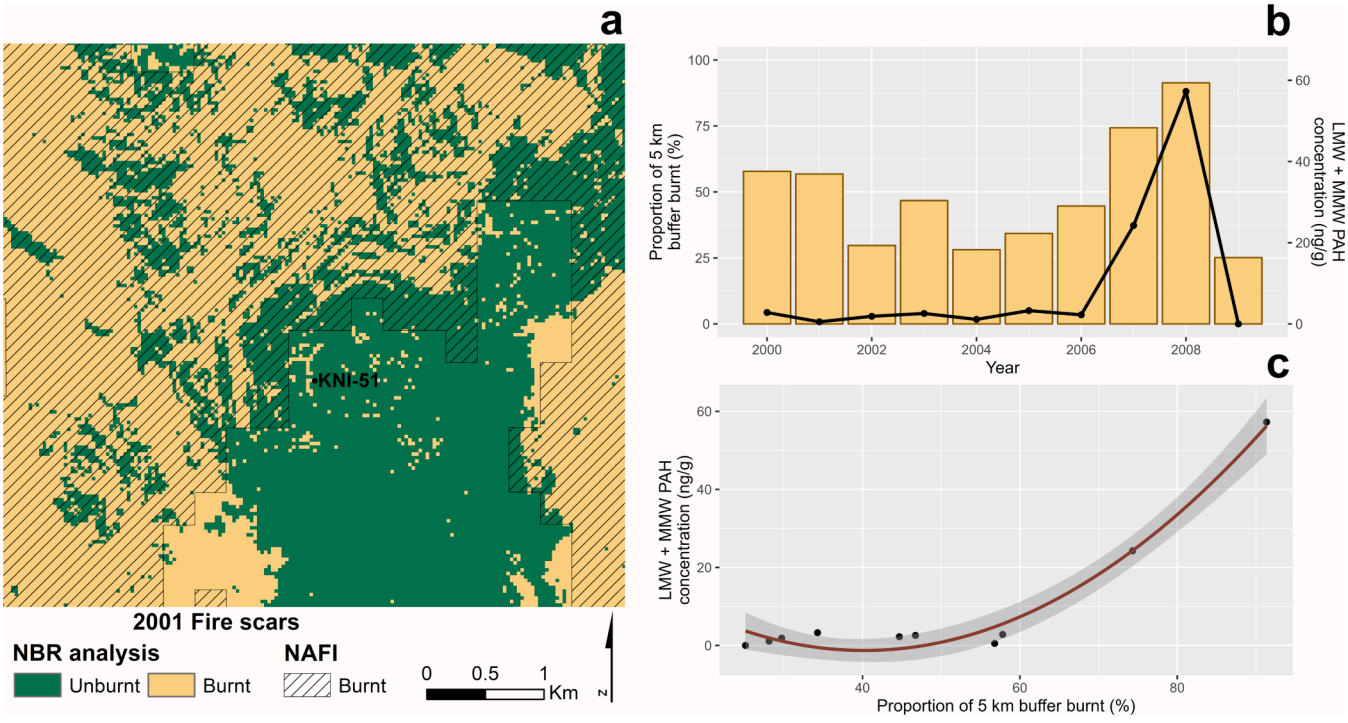

Fig. 11. Results of the fire severity analysis and comparison with LMW and MMW PAH concentration. (**a**) Example of the difference between fire scars as provided by NAFI (resolution 250 m) and those obtained in this study using Landsat imagery (resolution 30 m) for the year 2001. (**b**) Proportion of 5 km buffer burnt (orange bars) and concentration of LMW and MMW PAHs for each investigated year (black line). (**c**) Quadratic regression line between the proportion of area burnt and concentration of LMW + MMW PAHs within 5 km from KNI-51, which was selected as best model through AICc model selection (adjusted-$R^2 = 0.97$, p value = 2.4×10^{-6}). Grey shading represents the confidence interval.

be the source rock for the gas reservoir (Fig. S9). The Ningbing limestone outcrops only in a narrow NNE-oriented area, ranging in thickness from 171 to 1166 m (Mory and Beere, 1988; Earl, 2004; Gorter et al., 2004). Well completion reports including geochemical data are accessible through the Petroleum & Geothermal Information Management System (WAPIMS, https://wapims.dmp.wa.gov.au), although no detailed information about the hydrocarbon composition of oil shows is reported. Edwards et al. (1997) observed that oils from this sub-system reveal an algal and bacterial marine origin inferred from the biomarker and isotopic composition, although lower pristane/phytane ratio (Peters et al., 2004) and higher abundance of waxy (long-chain) *n*-alkanes at *Waggon Creek 1* suggest a contribution from land plants or higher thermal maturity. Petroleum types vary widely in the hydrocarbon composition as a result of their origin and maturation processes, including also numerous species (e.g., alkylated PAHs) often used for petroleum fingerprinting (Wang et al., 2012) that were not detected in samples from cave KNI-51. Thus, despite the proximity of the cave to oil shows and the complexity of a thorough comparison with our data, hydrocarbon leaks to the cave are reasonably an unlikely source of the observed organic compounds analyzed here, as supported by the lack of alkylated species in our chromatograms.

Alternative explanations for low CPI values include plant composition, microbiological activity, and thermal decomposition from burning. CPIs for single plant species vary naturally across a wide range (Bush and Mclnerney, 2013). For instance, graminoids - herbaceous, grass-like plants - constitute a large part of the tropical Australian savanna and have very low CPI values compared to woody angiosperms. Additionally, in Australia, soil CPIs were found to be lower than predicted values based on plant *n*-alkane composition, possibly as a result of post-depositional degradation (Howard et al., 2018). Kuhn et al. (2010) argue that the OEP pattern is typical of northern hemisphere sites, where most research has been conducted. Thus, the dry and warm conditions characterizing tropical savannas may result in a different observed *n*-alkane profile, as a product of the composition of the plant community and adaptation strategies.

Despite nutrient limitations, bacterial communities that rely on allochthonous organic matter flourish in caves and the literature provides wide evidence of microbially-mediated speleothem deposition (Barton and Northup, 2007; Blyth and Frisia, 2008; Bindschedler et al., 2016; Zhu et al., 2019). Several microorganisms including bacteria, fungi, and algae are capable of synthesizing alkanes or using them as a growth substrate (Ladygina et al., 2006; Wentzel et al., 2007). The abundance of the short-chain C_{15} and C_{17} *n*-alkanes, here detected in the soil, stalagmite mud layers, and stalagmite aragonite, is common to cyanobacteria (Valentine and Reddy, 2015) that, together with algal species, are reported to form biofilms on cave walls and ceilings (Czerwik-Marcinkowska and Mrozińska, 2011; Czerwik-Marcinkowska et al., 2015; Popović et al., 2015) and are the main photosynthetic component of biological soil crusts, widespread across Australia (Williams et al., 2014). Xie et al. (2003) attributed a similar pattern of single *n*-alkanes and low CPI in a cave in subtropical southern China to the input from parent soil and microorganisms, wherein microbial reworking and the occurrence of even compounds in plant roots can affect the distribution.

Here, the most likely interpretation for the low CPI is the dominant contribution of recurrent savanna fires affecting the distribution through the thermal breakdown of *n*-alkane molecules by shifting it towards short-chain and even carbon numbers, as reported in literature (Kuhn et al., 2010; De la Rosa et al., 2012; Vicente et al., 2017; Sarangi et al., 2022) and further discussed below. For instance, the impact of burning on alkane distributions is evident in analyses of organic compounds in smoke from fires in Portugal (Vicente et al., 2017). This study revealed the presence of odd and even numbered *n*-alkanes, which was attributed primarily to plant epicuticular waxes. However, the CPI for these samples was always around 1, evidencing the lack of the typical plant OEP and resembling the pattern usually observed in microbial and fossil lipids. Thus, the fires drove thermally-induced breakdown and rearrangement of carbon chains, resulting in a wide variety of organic structures including shorter and/or even aliphatic and aromatic hydrocarbons such as PAHs. Similarly, Sarangi et al. (2022) performed a controlled burning of leaves and soil samples and found that burning above 300 °C resulted in significant lowering of TOC and CPI values of tree and shrub samples considered.

In conclusion, we consider *n*-alkanes in speleothems from cave KNI-51 as resulting from local processes related to surface vegetation and *in-situ* degradation from fire and, possibly, bacterial activity, as supported by the coherence between soil and speleothem distributions observed and the results from the library search of peaks obtained by full scan analysis.

4.3. Cave soil and stalagmite flood layers

The PAH composition of soil samples and stalagmite mud layers reflects the frequent bush fire activity in the area surrounding KNI-51. All PAH compounds detected here are fire-related and were also reported in gaseous and particulate emissions from the combustion of Western Australia woods and grasses (Zou et al., 2003; Dong et al., 2020) and in smoke from biomass burned during the 1997 prolonged fires in Indonesia (Fang et al., 1999). Overall, concentrations of PAHs are in line with those reported by Wilcke et al. (2002) in seasonally flooded tropical soils not impacted by anthropogenic activity in Brazil. Low concentrations of LMW and MMW PAHs suggest that soils were affected by volatilization, washout, and/or photochemical degradation (Kim et al., 2011; Choi, 2014) or microbial degradation ((Johnsen and Karlson, 2005). However, the relative abundance of naphthalene is not completely consistent with patterns generated by Australian combusted grasses, where naphthalene emission factors (amount of compound emitted per amount of biomass burned) are 1–2 orders of magnitude lower than 4- and 5-ring PAHs (Dong et al., 2020). Soil naphthalene levels were found to be very high after forest fires in South Korea and China, although accompanied by similar phenanthrene maxima (Kim et al., 2011; Choi, 2014). High levels of naphthalene and, to a lesser extent, phenanthrene and perylene in tropical soils were associated to biological sources. For instance, termites of the *Nasutitermes* genus and associated gut microorganisms, were proposed as a possible significant source of naphthalene in the Amazon (Wilcke et al., 2002; Krauss et al., 2005). Perylene was shown to be produced by wood degrading fungi and by fungus combs of termite nests, as a result of lignin degradation. Termites are common in mounds and tree hollows of Australian eucalypt savannas playing a significant role in organic carbon remineralization by decomposing wood and grass (Hill, 1942; Holt and Coventry, 1990; Dawes-Gromadzki, 2008; ALA, 2022) and are regarded as one of the main woody vegetation disturbance factors together with cyclones and fire (Werner and Prior, 2007; Woolley et al., 2018). Although no precise estimates are available, they are abundant in the cave region, hence a possible role of termites in affecting the soil load of PAHs should thus be considered both as a positive contribution to the naphthalene stock and as a potential actor in the degradation of other compounds. Nonetheless, fire remains the dominant source of LMW and MMW PAHs in the tropics and in the cave area.

The distribution of *n*-alkanes in stalagmite mud layers is clearly bimodal with maxima at C_{15}-C_{16} and C_{27}-C_{30}. Concentrations are normally distributed in the C_{23}-C_{35} interval, an occurrence common to plant-derived aliphatic hydrocarbons. *n*-Alkanes in this range are commonly found in particulates from biomass burning and carbonaceous combustion residues, both during and after wildfire events (and in controlled experiments). As an effect of thermal alteration, observed profiles often lose the features of vegetation characterized by a marked odd over even predominance, resulting in CPIs as low as 1–2 and shifts of the maximum in the distribution towards lower carbon chains (Fang et al., 1999; Simoneit, 2002; Fernandes and Brooks, 2003; Vicente et al., 2017). The alkane profile observed in stalagmite mud layers samples is similar to vegetation fire residues collected after controlled burning of

native vegetation in Victoria, Australia, and straw charcoal obtained from pea straw (Fernandes and Brooks, 2003). Simoneit (2002) reports higher CPIs for smoke from combusted grasses (11.8) compared to angiosperms (2.6) and gymnosperms (1.2). Such occurrence in fire residues might be used as diagnostic of the dominant type of fuel, although combustion conditions can largely affect distributions and emission factors.

Concentrations of PAHs in stalagmite mud layers were approximately 1–2 orders of magnitude higher than soil values, mainly due to LMW PAHs (mostly absent in soil samples except for naphthalene). A similar occurrence was observed for *n*-alkanes. This suggests that compounds contained in stalagmite flood layers are preserved from degradation, in contrast to tropical soils that experience vaporization and leaching.

4.4. Stalagmite aragonite

As with flood layers, more compounds are preserved in stalagmite aragonite than in soil samples, suggesting a similar interpretation in terms of preservation. Overall, concentrations of PAHs in stalagmite aragonite are similar to or slightly lower than those in cave sediment samples, suggesting the latter is unlikely as a secondary source of organic compounds. Correlation analysis further suggests that the occurrence of PAHs in speleothems is not significantly affected by the composition of sediments and the frequency of flood events.

The transfer of PAHs to the cave system is likely affected only minimally by soil adsorption or fractionation in the thin overlying soil, and the intense monsoon rainfall regime makes transport via infiltrating fluids the dominant source of PAHs in stalagmites (a controlled burn and irrigation experiment will soon be conducted to quantify these effects). Our data suggest short residence times for LMW and MMW PAHs in soil over the cave, implying that PAHs in stalagmites might better serve to reconstruct fires occurring in the late dry season, closer in time to the wet season where infiltration and cave flooding mostly occur. Such fires are often characterized by higher burning temperatures than fires earlier in the dry season owing to drier fuel, increased litter amount, and hotter and drier atmospheric conditions (Williams et al., 1998).

Stalagmite KNI-51-F presents higher levels of HMW compounds than KNI-51-11 and KNI-51-G. This might be ascribable to a higher frequency of flood layers compared to KNI-51-11 and KNI-51-G (flood layers/total layers counted = 0.20 for KNI-11-F, 0.12 for KNI-51-G, and 0.13 for KNI-51-11), the chemical evolution of these compounds along different infiltration pathways, or differences in fuel composition.

4.5. Association with fire occurrence and ecological implications

The comparison of PAH concentrations with the extent of fires in proximity of KNI-51 showed a positive correlation only at a landscape scale, with the proportion of burned land associated with increase in the concentration of LMW and MMW PAHs only within the wider buffers (1–5 km; Fig. S8). Consistently, the higher PAH concentrations were observed only when a substantial (>60 %) proportion of the examined area was burned, regardless of its size (Fig. 11b), indicating that PAH concentration best reflects extensive fires affecting a substantial portion of the landscape. This suggests that PAHs in stalagmites could provide ecologically valuable insights into fire activity, filling important gaps in our understanding of the fire history of the area. It is widely accepted that European colonization and the subsequent impacts on Aboriginal burning practices led to shifts in fire regimes in northern Australia, with an increase in large-scale, high-intensity fires (Russell-Smith et al., 2003) that altered vegetation structure and forced the decline of fire-sensitive species (Prior et al., 2011). A more comprehensive understanding of paleofire regimes will contribute to disentangling the effects of climate variability and anthropogenic influences on fire activity in the region (Lynch et al., 2007), informing fire management and conservation programs.

While these results are promising, caution is needed in interpreting them due to the sample size available, which likely affected the high adjusted-R^2 and very low p value obtained with our analysis. Although PAH data span a wide temporal range, the comparison of PAH concentration with fire scars was restricted to fires between 2000 and 2009. Previous research on the use of satellite images to detect fire severity has shown that the timing of the post-fire images affects the quality of the outputs (Holden et al., 2005). Further, the fires detected in this study were predominantly of low severity, from which the local fire-adapted savannas and eucalypt woodlands would likely recover quickly (Ondei et al., 2016), potentially masking fire-severity signals detectable from satellite imagery (Bowman et al., 2003). To account for this, we limited our comparison of fire scars and PAH concentrations to those years when the dates of fires occurring within 5 km of the cave were known in order to select imagery captured shortly after the fires. Since the NASA Terra satellite, whose Moderate Resolution Imaging Spectroradiometer (MODIS) is used by NAFI to provide information on time and extent of fires in northern Australia, was launched in 2000 (https://terra.nasa.gov/), it is not possible to know the time of fire occurrence prior to that date. While this choice limited the temporal range of our spatial analyses, it also allowed us to minimize potential confounding factors caused by inaccuracies in the analyses. Future research should investigate the interplay between proportion of burned land, fire severity and intensity, and PAH accumulation dynamics using a broader range of remote sensing records and analytical methods (Williamson et al., 2022).

5. Conclusions

The purpose of this work is to provide a framework for high resolution paleofire reconstruction from well-dated, fast-growing aragonite stalagmites. Cave KNI-51 appears well suited for this approach due to the precise radiometric dates and high temporal resolution afforded by its stalagmites, the thin overlying soils, and the high frequency of bushfires. PAH abundances in three stalagmites retrieved from cave KNI-51 have been described so far. Analysis of stalagmite aragonite, flood sediment included in stalagmites, sediment samples from the cave floor, and soils from above the cave suggest negligible contamination from included sediments or sample processing, supporting the validity of stalagmite PAHs as paleofire proxies. Furthermore, the agreement between coeval stalagmites, as well as the positive association between PAHs and the presence of fires in the landscape surrounding the cave validate the application of our method. Improving our knowledge of paleofire activity is critical to infer background rates of bush fire and allow an examination of climate and anthropogenic influences (Bowman et al., 2022; Shuman et al., 2022). This proposed novel approach has the potential to greatly expand the temporal range and resolution of the existing paleofire records in areas where other suitable cave systems can be found.

Declaration of competing interest

The authors declare that they have no known competing financial interests or personal relationships that could have appeared to influence the work reported in this paper.

Data availability

Data are available through Mendeley Data at https://doi.org/10.17632/zpmjwkcnrz.1.

Acknowledgements

We gratefully acknowledge assistance in Kununurra and KNI-51 by Donna Cavlovic and Steve Stevets. We also gratefully acknowledge the Miriuwung Gajerrong people and the owners and leaseholders of Carlton

Hill Station.

This work was supported by U.S. National Science Foundation Division of Environmental Biology (grant numbers 1812476 and 2147186) and the Paleo Perspective on Climate Change program (grant numbers 1502917 and 1602544), Cornell College, the Institute of Polar Sciences, and Ca' Foscari University.

Appendix A. Supplementary material

Supplementary material file contains details on: (i) relative humidity at KNI-51, (ii) age models of the three stalagmites, (iii) sampling of soil and cave sediment samples, (iv) GC-MS/MS parameters used for PAH analysis, (v) sequential digestion, (vi) elemental analysis data, (vii) occurrence of non-pyrogenic organic compounds in chromatograms, (viii) *n*-alkanes distribution in thick sediment samples, (ix) occurrence of low and moderate severity fires in buffers and years used for the association of PAH concentrations with fire scars, and (x) petroleum deposits distribution around KNI-51. Supplementary material to this article can be found online at https://doi.org/10.1016/j.gca.2023.11.033.

References

Ahmad, M., Munson, T., 2012. Geology and Mineral Resources Resources of the Northern Territory. In: Northern Territory Geological Survey Special Publication 5 Northern Territory Government.

Atlas of living Australia, 2022. *family: TERMITIDAE*, accessed 2022-02-16, https://biocache.ala.org.au/occurrence/search?q=lsid%3Aurn%3Alsid%3Abiodiversity.org.au%3Aafd.taxon%3A3eacb1a9-e519-4f25-9bdb-218572aa7dac&qualityProfile=ALA.

Alcaras, E., Costantino, D., Guastaferro, F., Parente, C., Pepe, M., 2022. Normalized Burn Ratio Plus (NBR+): a new index for Sentinel-2 imagery. Remote Sens. 14.

Argiriadis, E., Battistel, D., McWethy, D.B., Vecchiato, M., Kirchgeorg, T., Kehrwald, N. M., Whitlock, C., Wilmshurst, J.M., Barbante, C., 2018. Lake sediment fecal and biomass burning biomarkers provide direct evidence for prehistoric human-lit fires in New Zealand. Sci. Rep. 8, 12113.

Argiriadis, E., Denniston, R.F., Barbante, C., 2019. Improved polycyclic aromatic hydrocarbons and n-alkanes determination in speleothems through cleanroom sample processing. Anal. Chem. 91, 7007–7011.

Australia, G., 2021. Regional geology of the bonaparte basin. Reg. Geol. Bonaparte Basin.

Barton, H.A., Northup, D.E., 2007. Geomicrobiology in cave environments: Past, current and future perspectives. J. Cave Karst Stud. 69, 163–178.

Bartoń, K., 2023. MuMIn: Multi-Model Inference. R package version 1.47.5. https://CRAN.R-project.org/package=MuMIn.

Bindschedler, S., Cailleau, G., Verrecchia, E., 2016. Role of Fungi in the Biomineralization of Calcite. Minerals 6, 41.

Bivand, R., Keitt, T., Rowlingson, B., 2023. rgdal: Bindings for the Geospatial Data Abstraction Library. R package version 0.9-1.

Blyth, A.J., Farrimond, P., Jones, M., 2006. An optimised method for the extraction and analysis of lipid biomarkers from stalagmites. Org. Geochem. 37, 882–890.

Blyth, A.J., Baker, A., Collins, M.J., Penkman, K.E.H., Gilmour, M.A., Moss, J.S., Genty, D., Drysdale, R.N., 2008. Molecular organic matter in speleothems and its potential as an environmental proxy. Quat. Sci. Rev. 27, 905–921.

Blyth, A.J., Frisia, S., 2008. Molecular evidence for bacterial mediation of calcite formation in cold high-altitude caves. Geomicrobiol. J. 25, 101–111.

Blyth, A.J., Hartland, A., Baker, A., 2016. Organic proxies in speleothems - New developments, advantages and limitations. Quat. Sci. Rev. 149, 1–17.

Bowman, D.M.J.S., Balch, J.K., Artaxo, P., Bond, W.J., Carlson, J.M., Cochrane, M.A., D'Antonio, C.M., Defries, R.S., Doyle, J.C., Harrison, S.P., Johnston, F.H., Keeley, J. E., Krawchuk, M.A., Kull, C.A., Marston, J.B., Moritz, M.A., Prentice, I.C., Roos, C.I., Scott, A.C., Swetnam, T.W., van der Werf, G.R., Pyne, S.J., 2009. Fire in the Earth system. Science 324, 481–484.

Bowman, D.M.J.S., Williamson, G.J., Johnston, F.H., Bowman, C.J.W., Murphy, B.P., Roos, C.I., Trauernicht, C., Rostron, J., Prior, L.D., 2022. Population collapse of a Gondwanan conifer follows the loss of Indigenous fire regimes in a northern Australian savanna. Sci. Rep. 12, 1–17.

Bowman, D.M., Zhang, Y., Walsh, A., Williams, R.J., 2003. Experimental comparison of four remote sensing techniques to map tropical savanna fire-scars using Landsat-TM imagery. Int. J. Wildland Fire 12, 341–348.

Brocks, J.J., Grosjean, E., Logan, G.A., 2008. Assessing biomarker syngeneity using branched alkanes with quaternary carbon (BAQCs) and other plastic contaminants. Geochim. Cosmochim. Acta 72, 871–888.

Bureau of Meteorology, 2023. Fire weather seasons, accessed 2023-11-27, http://www.bom.gov.au/weather-services/fire-weather-centre/fire-weather-season/.

Burnham, K., Anderson, D., 2002. Model Selection and Multimodel Inference: A Practical Information-Theoretic Approach, second ed. Springer, New York, New York, USA.

Bush, R.T., McInerney, F., 2013. Leaf wax n-alkane distributions in and across modern plants: Implications for paleoecology and chemotaxonomy. Geochim. Cosmochim. Acta 117, 161–179.

Campbell, M., McDonough, L., Treble, P.C., Baker, A., Kosarac, N., Coleborn, K., Wynn, P.M., Schmitt, A.K., 2023. A review of speleothems as archives for paleofire proxies, with Australian case studies. Rev. Geophys. 61, 1–35.

Castañeda, I.S., Schouten, S., 2011. A review of molecular organic proxies for examining modern and ancient lacustrine environments. Quat. Sci. Rev. 30, 2851–2891.

Chen, X., Hutley, L.B., Eamus, D., 2005. Soil organic carbon content at a range of north Australian tropical savannas with contrasting site histories. Plant Soil 268, 161–171.

Cheng, Y.Y., Yu, J.Z., 2020. Minimizing contamination from plastic labware in the quantification of c16 and c18 fatty acids in filter samples of atmospheric particulate matter and their utility in apportioning cooking source contribution to urban pm2.5. Atmosphere (Basel) 11.

Choi, S., 2014. Time trends in the levels and patterns of polycyclic aromatic hydrocarbons (PAHs) in pine bark, litter, and soil after a forest fire. Sci. Total Environ. 470–471, 1441–1449.

Cisneros, M., Cacho, I., Moreno, A., Stoll, H., Torner, J., Català, A., Edwards, R.L., Cheng, H., Fornós, J.J., 2021. Hydroclimate variability during the last 2700 years based on stalagmite multi-proxy records in the central-western Mediterranean. Quat. Sci. Rev. 269, 107137.

Countway, R.E., Dickhut, R.M., Canuel, E.A., 2003. Polycyclic aromatic hydrocarbon (PAH) distributions and associations with organic matter in surface waters of the York River, VA Estuary. Org. Geochem. 34, 209–224.

Czerwik-Marcinkowska, J., Mrozińska, T., 2011. Algae and cyanobacteria in caves of the Polish Jura. Polish Bot. J. 56, 203–243.

Czerwik-Marcinkowska, J., Wojciechowska, A., Massalski, A., 2015. Biodiversity of limestone caves: aggregations of aerophytic algae and cyanobacteria in relation to site factors. Polish J. Ecol. 63, 481–499.

Dawes-Gromadzki, T.Z., 2008. Abundance and diversity of termites in a savanna woodland reserve in tropical Australia. Aust. J. Entomol. 47, 307–314.

De la Rosa, J.M., Faria, S.R., Varela, M.E., Knicker, H., González-Vila, F.J., González-Pérez, J.A., Keizer, J., 2012. Characterization of wildfire effects on soil organic matter using analytical pyrolysis. Geoderma 191, 24–30.

Denniston, R.F., Villarini, G., Gonzales, A.N., Wyrwoll, K.-H., Polyak, V.J., Ummenhofer, C.C., Lachniet, M.S., Wanamaker, A.D., Humphreys, W.F., Woods, D., Cugley, J., 2015. Extreme rainfall activity in the Australian tropics reflects changes in the El Niño/Southern Oscillation over the last two millennia. Proc. Natl. Acad. Sci. 112, 4576–4581.

Denniston, R.F., Ummenhofer, C.C., Wanamaker, A.D., Lachniet, M.S., Villarini, G., Asmerom, Y., Polyak, V.J., Passaro, K.J., Cugley, J., Woods, D., Humphreys, W.F., 2016. Expansion and Contraction of the Indo-Pacific Tropical Rain Belt over the Last Three Millennia. Sci. Rep. 6, 34485.

Department of the Environment and Energy, 2020. National Vegetation Information System (NVIS) Version 6.0 – Australia – extant vegetation.

Dong, T.T.T., Stock, W.D., Callan, A.C., Strandberg, B., Hinwood, A.L., 2020. Emission factors and composition of PM2.5 from laboratory combustion of five Western Australian vegetation types. Sci. Total Environ. 703, 134796.

Dorale, J.A., Liu, Z., 2009. Limitations of hendy test criteria in judging the paleoclimatic suitability of speleothems and the need for replication. J. Cave Karst Stud. 71, 73–80.

Duan, W., Ruan, J., Luo, W., Li, T., Tian, L., Zeng, G., Zhang, D., Bai, Y., Li, J., Tao, T., Zhang, P., Baker, A., Tan, M., 2016. The transfer of seasonal isotopic variability between precipitation and drip water at eight caves in the monsoon regions of China. Geochim. Cosmochim. Acta 183, 250–266.

Earl, K.L., 2004. The petroleum systems of the bonaparte basin. Geosci. Aust. GEOCAT 61.

Eckmeier, E., Wiesenberg, G.L.B., 2009. Short-chain n -alkanes (C16–20) in ancient soil are useful molecular markers for prehistoric biomass burning. J. Archaeol. Sci. 36, 1590–1596.

Edwards, D.S., Summons, R.E., Kennard, J.M., Nicoll, R.S., Bradshaw, J., Bradshaw, M., Foster, C.B., O'Brien, G.W., Zumberge, J.E., 1997. Geochemical Characteristics of Palaeozoic Petroleum Systems in Northwestern Australia. APPEA J. 37, 351.

Fairchild, I.J., Treble, P.C., 2009. Trace elements in speleothems as recorders of environmental change. Quat. Sci. Rev. 28, 449–468.

Fang, M., Zheng, M., Wang, F., To, K.L., Jaafar, A.B., Tong, S.L., 1999. The solvent-extractable organic compounds in the Indonesia biomass burning aerosols — characterization studies. Atmos. Environ. 33.

Fernandes, M.B., Brooks, P., 2003. Characterization of carbonaceous combustion residues: II nonpolar organic compounds. Chemosphere 53, 447–458.

Gorter, J.D., McKirdy, D.M., Jones, P.J., Playford, G., 2004. Reappraisal of the Early Carboniferous Milligans Formation source rock system in the southern Bonaparte Basin, northwestern Australia. Timor Sea Pet. Geosci. Proc. Timor Sea Symp. Darwin 2003, 231–255.

Hijmans, R.J., 2020. raster: Geographic Data Analysis and Modeling. R package version 2.5-8. https://CRAN.R-project.org/package=raster.

Hill G.F., 1942. Termites (Isoptera) from the Australian region. Commonwealth of Australia. Council for Scientific and Industrial Research.

Holden, Z.A., Smith, A.M.S., Morgan, P., Rollins, M.G., Gessler, P.E., 2005. Evaluation of novel thermally enhanced spectral indices for mapping fire perimeters and comparisons with fire atlas data. Int. J. Remote Sens. 26, 4801–4808.

Holt, J.A., Coventry, R.J., 1990. Nutrient cycling in Australian savannas. J. Biogeogr. 17, 427–432.

Homann, J., Oster, J.L., Wortham, B.E., Breitenbach, S.F.M., Hoffman, T., 2022. Linked fire activity and climate whiplash in California during the early Holocene. Nat. Commun. 13, 7175.

Homann, J., Karbach, N., Carolin, S.A., James, D.H., Hodell, D., Breitenbach, S.F.M., Kwiecien, O., Brenner, M., Peraza, L.C., Hoffmann, T., 2023. Past fire dynamics inferred from polycyclic aromatic hydrocarbons and monosaccharide anhydrides in

a stalagmite from the archaeological site of Mayapan, Mexico. Biogeosciences 20, 3249–3260.
Howard, S., McInerney, F.A., Caddy-Retalic, S., Hall, P.A., Andrae, J.W., 2018. Modelling leaf wax n-alkane inputs to soils along a latitudinal transect across Australia. Org. Geochem. 121, 126–137.
Johnsen, A.R., Karlson, U., 2005. PAH degradation capacity of soil microbial communities—Does it depend on PAH exposure? Microb. Ecol. 50, 488–495.
Kaal, J., Martínez-Pillado, V., Martínez, C.A., Sanjurjo-Sánchez, J., Aranburu, A., Arsuaga, J.L., Iriarte, E., 2021. Bacteria, guano and soot: Source assessment of organic matter preserved in black laminae in stalagmites from caves of the sierra de atapuerca (N Spain). Int. J. Speleol. 50, 121–135.
Kehrwald, N., Zangrando, R., Gambaro, A., Barbante, C., 2010. Fire and climate: Biomass burning recorded in ice and lake cores. EPJ Web Conf. 9, 105–114.
Kim, E.J., Choi, S., Chang, Y., 2011. Levels and patterns of polycyclic aromatic hydrocarbons (PAHs) in soils after forest fires in South Korea. Environ. Sci. Pollut. Res. 18, 1508–1517.
Krauss, M., Wilcke, W., Martius, C., Bandeira, A.G., Garcia, M.V.B., Amelung, W., 2005. Atmospheric versus biological sources of polycyclic aromatic hydrocarbons (PAHs) in a tropical rain forest environment. Environ. Pollut. 135, 143–154.
Kuhn, T.K., Krull, E.S., Bowater, A., Grice, K., Gleixner, G., 2010. The occurrence of short chain n-alkanes with an even over odd predominance in higher plants and soils. Org. Geochem. 41, 88–95.
Lachniet, M.S., 2009. Climatic and environmental controls on speleothem oxygen-isotope values. Quat. Sci. Rev. 28, 412–432.
Ladygina, N., Dedyukhina, E.G., Vainshtein, M.B., 2006. A review on microbial synthesis of hydrocarbons. Process Biochem. 41, 1001–1014.
Lasslop, G., Coppola, A.I., Voulgarakis, A., Yue, C., Veraverbeke, S., 2019. Influence of fire on the carbon cycle and climate. Curr. Clim. Chang. Reports 5, 112–123.
Lynch, A.H., Beringer, J., Kershaw, P., Marshall, A., Mooney, S., Tapper, N., Turney, C., Van Der Kaars, S., 2007. Using the paleorecord to evaluate climate and fire interactions in Australia. Annu. Rev. Earth Planet. Sci. 35, 215–239.
Margolis, E.Q., Guiterman, C.H., Chavardès, R.D., Coop, J.D., Copes-Gerbitz, K., Dawe, D.A., Falk, D.A., Johnston, J.D., Larson, E., Li, H., Marschall, J.M., Naficy, C. E., Naito, A.T., Parisien, M.-A., Parks, S.A., Portier, J., Poulos, H.M., Robertson, K.M., Speer, J.H., Stambaugh, M., Swetnam, T.W., Tepley, A.J., Thapa, I., Allen, C.D., Bergeron, Y., Daniels, L.D., Fulé, P.Z., Gervais, D., Girardin, M.P., Harley, G.L., Harvey, J.E., Hoffman, K.M., Huffman, J.M., Hurteau, M.D., Johnson, L.B., Lafon, C. W., Lopez, M.K., Maxwell, R.S., Meunier, J., North, M., Rother, M.T., Schmidt, M.R., Sherriff, R.L., Stachowiak, L.A., Taylor, A., Taylor, E.J., Trouet, V., Villarreal, M.L., Yocom, L.L., Arabas, K.B., Arizpe, A.H., Arseneault, D., Tarancón, A.A., Baisan, C., Bigio, E., Biondi, F., Cahalan, G.D., Caprio, A., Cerano-Paredes, J., Collins, B.M., Dey, D.C., Drobyshev, I., Farris, C., Fenwick, M.A., Flatley, W., Floyd, M.L., Gedalof, Z., Holz, A., Howard, L.F., Huffman, D.W., Iniguez, J., Kipfmueller, K.F., Kitchen, S.G., Lombardo, K., McKenzie, D., Merschel, A.G., Metlen, K.L., Minor, J., O'Connor, C.D., Platt, L., Platt, W.J., Saladyga, T., Stan, A.B., Stephens, S., Sutheimer, C., Touchan, R., Weisberg, P.J., 2022. The North American tree-ring fire-scar network. Ecosphere 13, e4159.
McDonough, L.K., Treble, P.C., Baker, A., Borsato, A., Frisia, S., Nagra, G., Coleborn, K., Gagan, M.K., Zhao, J.X., Paterson, D., 2022. Past fires and post-fire impacts reconstructed from a southwest Australian stalagmite. Geochim. Cosmochim. Acta 325, 258–277.
Mory, A., Beere, G., 1988. Geology of the onshore Bonaparte and Ord Basins in Western Australia. GSWA Bull. 134, 1–200.
Ondei, S., Prior, L.D., Vigilante, T., Bowman, D.M.J.S., 2016. Post-fire resprouting strategies of rainforest and savanna saplings along the rainforest–savanna boundary in the Australian monsoon tropics. Plant Ecol. 217, 711–724.
Oros, D.R., Simoneit, B.R.T., 2001. Identification and emission factors of molecular tracers in organic aerosols from biomass burning Part 2. Deciduous Trees. Appl. Geochem. 16, 1545–1565.
Perrette, Y., Poulenard, J., Saber, A.-I., Fanget, B., Guittonneau, S., Ghaleb, B., Garaudee, S., 2008. Polycyclic Aromatic Hydrocarbons in stalagmites: occurrence and use for analyzing past environments. Chem. Geol. 251, 67–76.
Peters, K.E., Walters, C.C., Moldowan, J.M., 2004. The Biomarker Guide, second ed. Cambridge University Press, Cambridge.
Philipp, M.B., Levick, S.R., 2020. Exploring the Potential of C-Band SAR in Contributing to Burn Severity Mapping in Tropical Savanna. Remote Sens. 12.
Pignatello, J.J., 1998. Soil organic matter as a nanoporous sorbent of organic pollutants. Adv. Colloid Interface Sci. 76–77, 445–467.
Popović, S., Simić, G.S., Stupar, M., Unković, N., Predojević, D., Jovanović, J., Grbić, M. L., 2015. Cyanobacteria, algae and microfungi present in biofilm from Božana Cave (Serbia). Int. J. Speleol. 44, 141–149.
Prior, L.D., McCaw, W.L., Grierson, P.F., Murphy, B.P., Bowman, D.M.J.S., 2011. Population structures of the widespread Australian conifer Callitris columellaris are a bio-indicator of continental environmental change. For. Ecol. Manage. 262, 252–262.
R Core Team, 2021. R: A Language and Environment for Statistical Computing.
R Core Team, 2023. R: A Language and Environment for Statistical Computing.
Ramseyer, K., Miano, T.M., D'Orazio, V., Wildberger, A., Wagner, T., Geister, J., 1997. Nature and origin of organic matter in carbonates from speleothems, marine cements and coral skeletons. Org. Geochem. 26, 361–378.
Rey-Salgueiro, L., Martínez-Carballo, E., Merino, A., Vega, J.A., Fonturbel, M.T., Simal-Gandara, J., 2018. Polycyclic aromatic hydrocarbons in soil organic horizons depending on the soil burn severity and type of ecosystem. L. Degrad. Dev. 2123, 2112–2123.
Russell-Smith, J., Yates, C., Edwards, A., Allan, G.E., Cook, G.D., Cooke, P., Craig, R., Heath, B., Smith, R., 2003. Contemporary fire regimes of northern Australia, 1997–2001: change since Aboriginal occupancy, challenges for sustainable management. Int. J. Wildl. Fire 12, 283–297.
Sarangi, V., Roy, S., Sanyal, P., 2022. Effect of burning on the distribution pattern and isotopic composition of plant biomolecules: implications for paleoecological studies. Geochim. Cosmochim. Acta 318, 305–327.
Shuman, J.K., Balch, J.K., Barnes, R.T., Higuera, P.E., Roos, C.I., Schwilk, D.W., Stavros, E.N., Banerjee, T., Bela, M.M., Bendix, J., Bertolino, S., Bililign, S., Bladon, K.D., Brando, P., Breidenthal, R.E., Buma, B., Calhoun, D., Carvalho, L.M.V., Cattau, M.E., Cawley, K.M., Chandra, S., Chipman, M.L., Cobian-Iñiguez, J., Conlisk, E., Coop, J.D., Cullen, A., Davis, K.T., Dayalu, A., De Sales, F., Dolman, M., Ellsworth, L.M., Franklin, S., Guiterman, C.H., Hamilton, M., Hanan, E.J., Hansen, W.D., Hantson, S., Harvey, B.J., Holz, A., Huang, T., Hurteau, M.D., Ilangakoon, N.T., Jennings, M., Jones, C., Klimaszewski-Patterson, A., Kobziar, L.N., Kominoski, J., Kosovic, B., Krawchuk, M.A., Laris, P., Leonard, J., Loria-Salazar, S. M., Lucash, M., Mahmoud, H., Margolis, E., Maxwell, T., McCarty, J.L., McWethy, D. B., Meyer, R.S., Miesel, J.R., Moser, W.K., Nagy, R.C., Niyogi, D., Palmer, H.M., Pellegrini, A., Poulter, B., Robertson, K., Rocha, A.V., Sadegh, M., Santos, F., Scordo, F., Sexton, J.O., Sharma, A.S., Smith, A.M.S., Soja, A.J., Still, C., Swetnam, T., Syphard, A.D., Tingley, M.W., Tohidi, A., Trugman, A.T., Turetsky, M., Varner, J.M., Wang, Y., Whitman, T., Yelenik, S., Zhang, X., 2022. Reimagine fire science for the anthropocene. PNAS Nexus 1, 1–14.
Simoneit, B.R.T., 2002. Biomass burning — a review of organic tracers for smoke from incomplete combustion. Appl. Geochem. 17, 129–162.
Smith, A.M.S., Drake, N.A., Wooster, M.J., Hudak, A.T., Holden, Z.A., Gibbons, C.J., 2007. Production of Landsat ETM+ reference imagery of burned areas within Southern African savannahs: comparison of methods and application to MODIS. Int. J. Remote Sens. 28, 2753–2775.
Stockmann, U., Padarian, J., McBratney, A., Minasny, B., de Brogniez, D., Montanarella, L., Hong, S.Y., Rawlins, B.G., Field, D.J., 2015. Global soil organic carbon assessment. Glob. Food Sec. 6, 9–16.
Sun, Y., Zhang, S., Lan, J., Xie, Z., Pu, J., Yuan, D., Yang, H., Xing, B., 2019. Vertical migration from surface soils to groundwater and source appointment of polycyclic aromatic hydrocarbons in epikarst spring systems, southwest China. Chemosphere 230, 616–627.
Ukalska-Jaruga, A., Smreczak, B., Klimkowicz-Pawlas, A., 2019. Soil organic matter composition as a factor affecting the accumulation of polycyclic aromatic hydrocarbons. J. Soils Sediments 19, 1890–1900.
Valentine, D.L., Reddy, C.M., 2015. Latent hydrocarbons from cyanobacteria. Proc. Natl. Acad. Sci. U.S.A. 112, 13434–13435.
Vergnoux, A., Malleret, L., Asia, L., Doumenq, P., Theraulaz, F., 2011. Impact of forest fires on PAH level and distribution in soils. Environ. Res. 111, 193–198.
Vicente, A., Calvo, A., Fernandes, A.P., Nunes, T., Monteiro, C., Pio, C., Alves, C., 2017. Hydrocarbons in particulate samples from wildfire events in central Portugal in summer 2010. J. Environ. Sci. (china) 53, 122–131.
Wang, C., Wang, Y., Herath, H.M.S.K., 2017. Polycyclic aromatic hydrocarbons (PAHs) in biochar – Their formation, occurrence and analysis: a review. Org. Geochem. 114, 1–11.
Wang, Z., Yang, C., Yang, Z., Hollebone, B., Brown, C.E., Landriault, M., Sun, J., Mudge, S.M., Kelly-Hooper, F., Dixon, D.G., 2012. Fingerprinting of petroleum hydrocarbons (PHC) and other biogenic organic compounds (BOC) in oil-contaminated and background soil samples. J. Environ. Monit. 14, 2367–2381.
Wentzel, A., Ellingsen, T.E., Kotlar, H.-K., Zotchev, S.B., Throne-Holst, M., 2007. Bacterial metabolism of long-chain n-alkanes. Appl. Microbiol. Biotechnol. 76, 1209–1221.
Werner, P.A., Prior, L.D., 2007. Tree-piping termites and growth and survival of host trees in savanna woodland of north Australia. J. Trop. Ecol. 23, 611–622.
Wickham, H., Averick, M., Bryan, J., Chang, W., McGowan, L.D.A., François, R., Yutani, H., 2019. Welcome to the Tidyverse. J. Open Source Software 4, 1686.
Wilcke, W., 2000. Polycyclic aromatic hydrocarbons (PAHs) in soil - A review. J. Plant Nutr. Soil Sci. 163, 229–248.
Wilcke, W., Krauss, M., Amelung, W., 2002. Carbon isotope signature of Polycyclic Aromatic Hydrocarbons (PAHs): evidence for different sources in tropical and temperate environments? Environ. Sci. Technol. 36, 3530–3535.
Williams, W.J., Büdel, B., Reichenberger, H., Rose, N., 2014. Cyanobacteria in the Australian northern savannah detect the difference between intermittent dry season and wet season rain. Biodivers. Conserv. 23, 1827–1844.
Williams, R.J., Gill, A.M., Moore, P.H.R., 1998. Seasonal changes in fire behaviour in a tropical savanna in Northern Australia. Int. J. Wildl. Fire 8, 227–239.
Williamson, G.J., Ellis, T.M., Bowman, D.M., 2022. Double-differenced dNBR: combining MODIS and Landsat imagery to map fine-grained fire MOSAICS in lowland Eucalyptus savanna in Kakadu National Park. Northern Australia. *Fire* 5, 160.
Woolley, L.A., Murphy, B.P., Radford, I.J., Westaway, J., Woinarski, J.C.Z., 2018. Cyclones, fire, and termites: the drivers of tree hollow abundance in northern Australia's mesic tropical savanna. For. Ecol. Manage. 419–420, 146–159.
Wynn, P.M., Brocks, J.J., 2014. A framework for the extraction and interpretation of organic molecules in speleothem carbonate. Rapid Commun. Mass Spectrom. 28, 845–854.
Xie, S., Yi, Y., Huang, J., Hu, C., Cai, Y., Collins, M., Baker, A., 2003. Lipid distribution in a subtropical southern China stalagmite as a record of soil ecosystem response to paleoclimate change. Quater. Res. 60 (3), 340–347.

Yang, Y., Zhang, N., Xue, M., Tao, S., 2010. Impact of soil organic matter on the distribution of polycyclic aromatic hydrocarbons (PAHs) in soils. Environ. Pollut. 158, 2170–2174.
Zhu, H.-Z., Zhang, Z.-F., Zhou, N., Jiang, C.-Y., Wang, B.-J., Cai, L., Liu, S.-J., 2019. Diversity, distribution and co-occurrence patterns of bacterial communities in a karst cave system. Front. Microbiol. 10, 1726.
Zou, L.Y., Zhang, W., Atkiston, S., 2003. The characterisation of polycyclic aromatic hydrocarbons emissions from burning of different firewood species in Australia. Environ. Pollut. 124, 283–289.